Prevailing-frequency approximation of the coupling ray theory for S waves

Luděk Klimeš & Petr Bulant

Department of Geophysics
Faculty of Mathematics and Physics
Charles University, Prague, Czech Republic

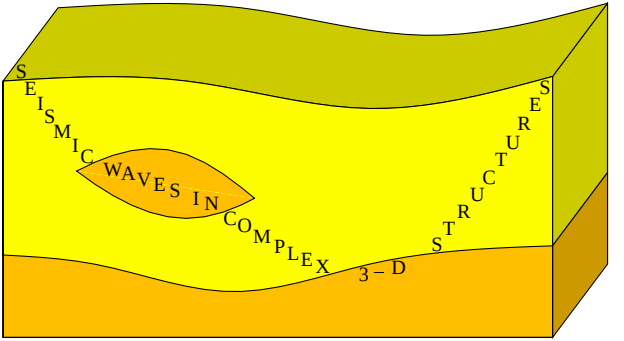

http://sw3d.cz

presented at 17th IWSA, Austin, Texas, September 20, 2016

Outline

Introduction to the coupling ray theory for S waves

Prevailing-frequency approximation of the coupling ray theory

Reference rays for the coupling ray theory

Generally anisotropic medium which is approximately transversely isotropic

SH and SV reference rays in a generally anisotropic medium

Interpolation of the coupling-ray-theory Green function within ray cells

Conclusions

Outline

Introduction to the coupling ray theory for S waves

Prevailing-frequency approximation of the coupling ray theory

Reference rays for the coupling ray theory

Generally anisotropic medium which is approximately transversely isotropic

SH and SV reference rays in a generally anisotropic medium

Interpolation of the coupling-ray-theory Green function within ray cells

Conclusions

Isotropic ray theory

Applicable to isotropic and very weakly anisotropic media.

Anisotropic ray theory

Always applicable to P waves.
Applicable to S waves in strongly anisotropic media.

Coupling ray theory for S waves (Coates & Chapman, 1990)

Applicable to isotropy and to all degrees of anisotropy.
Low-frequency limit: Isotropic ray theory.
High-frequency limit: Anisotropic ray theory.
Frequency-dependent S-wave polarization can be overcome
by the prevailing-frequency approximation (Klimeš & Bulant, 2012).
Calculated along the reference rays
which considerably influence the accuracy:
common S-wave reference rays, or SH and SV reference rays.

S-wave polarization along a ray:

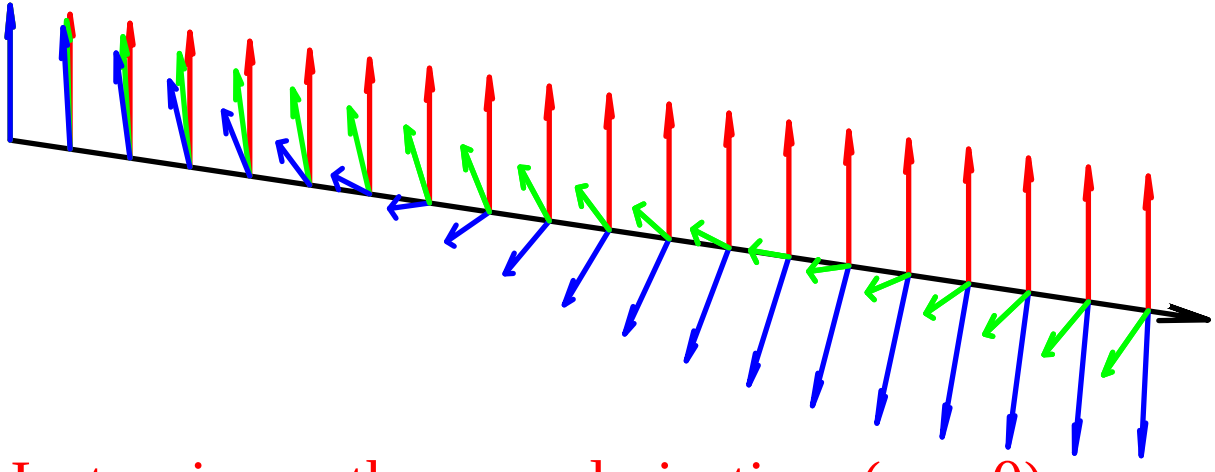

Isotropic ray theory polarization $(\omega = 0)$

Coupling ray theory polarization $(0 < \omega < \infty)$

Anisotropic ray theory polarization $(\omega = \infty)$

Comparison of isotropic, coupling and anisotropic ray theories in velocity model QIH

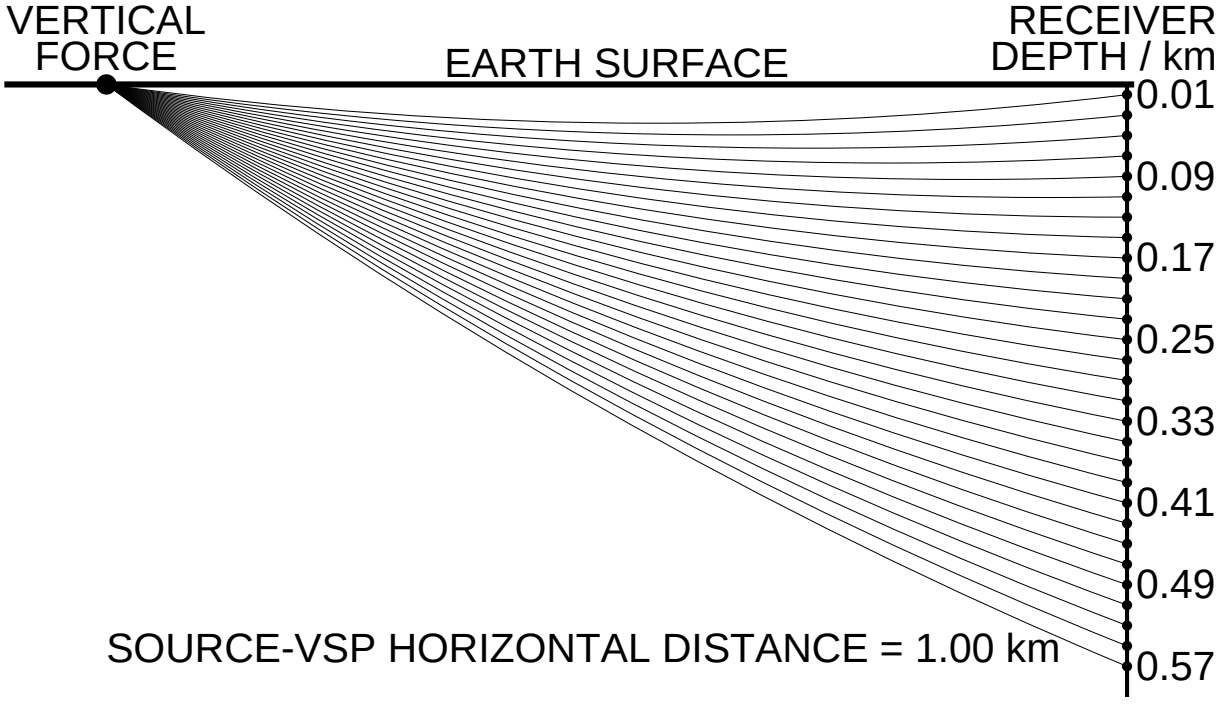

Density-normalized stiffness tensor in velocity model QIH

Depth of 0 km:

$$
\begin{array}{c}
 \\ 11 \\ 22 \\ 33 \\ 23 \\ 13 \\ 12
\end{array}
\begin{array}{c}
\begin{array}{cccccc} 11 & 22 & 33 & 23 & 13 & 12 \end{array} \\
\begin{pmatrix}
14.74250 & 4.66250 & 4.77500 & 0.00000 & 0.00000 & -0.29000 \\
 & 14.74250 & 4.77500 & 0.00000 & 0.00000 & -0.29000 \\
 & & 15.35500 & 0.00000 & 0.00000 & -0.14500 \\
 & & & 5.12750 & -0.08750 & 0.00000 \\
 & & & & 5.12750 & 0.00000 \\
 & & & & & 5.07250
\end{pmatrix}
\end{array}
$$

Depth of 1 km:

$$
\begin{array}{c}
 \\ 11 \\ 22 \\ 33 \\ 23 \\ 13 \\ 12
\end{array}
\begin{array}{c}
\begin{array}{cccccc} 11 & 22 & 33 & 23 & 13 & 12 \end{array} \\
\begin{pmatrix}
22.54482 & 7.16032 & 7.33187 & 0.00000 & 0.00000 & -0.44225 \\
 & 22.54482 & 7.33187 & 0.00000 & 0.00000 & -0.44225 \\
 & & 23.47887 & 0.00000 & 0.00000 & -0.22113 \\
 & & & 7.82569 & -0.13344 & 0.00000 \\
 & & & & 7.82569 & 0.00000 \\
 & & & & & 7.74182
\end{pmatrix}
\end{array}
$$

Coupling ray theory in model QIH (transverse component)

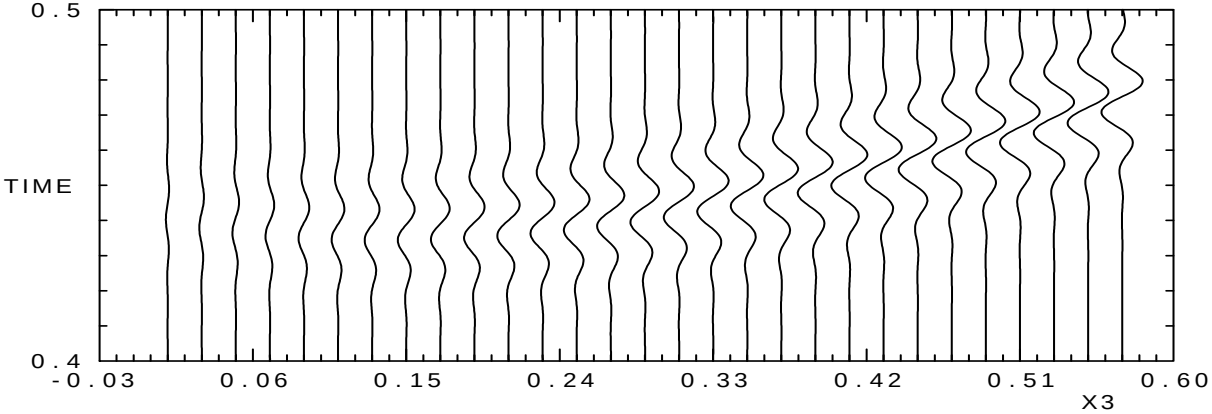

Anisotropic ray theory in model QIH (transverse component)

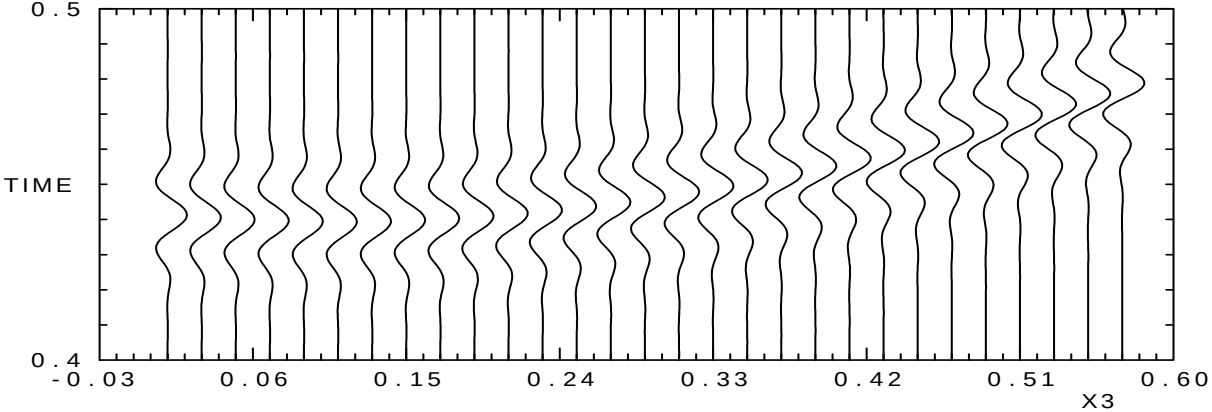

Development of S-wave splitting with increasing anisotropy in velocity models QIH, QI, QI2 and QI4 (anisotropy ratio 1 : 2 : 4 : 8)

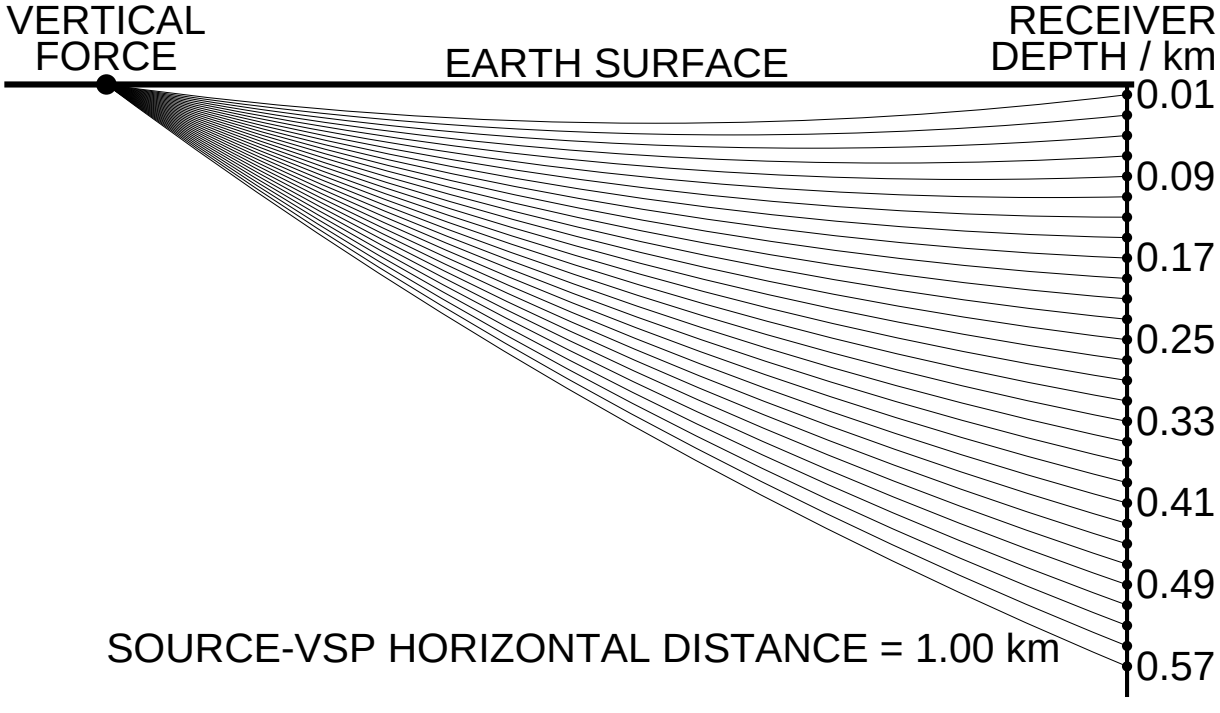

Density-normalized stiffness tensor in velocity model QI

Depth of 0 km:

$$
\begin{array}{c}
 \\ 11 \\ 22 \\ 33 \\ 23 \\ 13 \\ 12
\end{array}
\begin{array}{c}
\begin{array}{cccccc} 11 & 22 & 33 & 23 & 13 & 12 \end{array} \\
\begin{pmatrix}
14.48500 & 4.52500 & 4.75000 & 0.00000 & 0.00000 & -0.58000 \\
 & 14.48500 & 4.75000 & 0.00000 & 0.00000 & -0.58000 \\
 & & 15.71000 & 0.00000 & 0.00000 & -0.29000 \\
 & & & 5.15500 & -0.17500 & 0.00000 \\
 & & & & 5.15500 & 0.00000 \\
 & & & & & 5.04500
\end{pmatrix}
\end{array}
$$

Depth of 1 km:

$$
\begin{array}{c}
 \\ 11 \\ 22 \\ 33 \\ 23 \\ 13 \\ 12
\end{array}
\begin{array}{c}
\begin{array}{cccccc} 11 & 22 & 33 & 23 & 13 & 12 \end{array} \\
\begin{pmatrix}
22.08963 & 6.90063 & 7.24375 & 0.00000 & 0.00000 & -0.88450 \\
 & 22.08963 & 7.24375 & 0.00000 & 0.00000 & -0.88450 \\
 & & 23.95775 & 0.00000 & 0.00000 & -0.44225 \\
 & & & 7.86138 & -0.26688 & 0.00000 \\
 & & & & 7.86138 & 0.00000 \\
 & & & & & 7.69363
\end{pmatrix}
\end{array}
$$

Density-normalized stiffness tensor in velocity model QI2

Depth of 0 km:

$$
\begin{array}{c}
 \\ 11 \\ 22 \\ 33 \\ 23 \\ 13 \\ 12
\end{array}
\begin{array}{c}
\begin{array}{cccccc} 11 & 22 & 33 & 23 & 13 & 12 \end{array} \\
\begin{pmatrix}
13.97000 & 4.25000 & 4.70000 & 0.00000 & 0.00000 & -1.16000 \\
 & 13.97000 & 4.70000 & 0.00000 & 0.00000 & -1.16000 \\
 & & 16.42000 & 0.00000 & 0.00000 & -0.58000 \\
 & & & 5.21000 & -0.35000 & 0.00000 \\
 & & & & 5.21000 & 0.00000 \\
 & & & & & 4.99000
\end{pmatrix}
\end{array}
$$

Depth of 1 km:

$$
\begin{array}{c}
 \\ 11 \\ 22 \\ 33 \\ 23 \\ 13 \\ 12
\end{array}
\begin{array}{c}
\begin{array}{cccccc} 11 & 22 & 33 & 23 & 13 & 12 \end{array} \\
\begin{pmatrix}
21.17926 & 6.38126 & 7.06750 & 0.00000 & 0.00000 & -1.76900 \\
 & 21.17926 & 7.06750 & 0.00000 & 0.00000 & -1.76900 \\
 & & 24.91550 & 0.00000 & 0.00000 & -0.88450 \\
 & & & 7.93276 & -0.53376 & 0.00000 \\
 & & & & 7.93276 & 0.00000 \\
 & & & & & 7.59726
\end{pmatrix}
\end{array}
$$

Density-normalized stiffness tensor in velocity model QI4

Depth of 0 km:

$$
\begin{array}{c}
 \\ 11 \\ 22 \\ 33 \\ 23 \\ 13 \\ 12
\end{array}
\begin{array}{c}
\begin{array}{cccccc} 11 & 22 & 33 & 23 & 13 & 12 \end{array} \\
\begin{pmatrix}
12.94000 & 3.70000 & 4.60000 & 0.00000 & 0.00000 & -2.32000 \\
 & 12.94000 & 4.60000 & 0.00000 & 0.00000 & -2.32000 \\
 & & 17.84000 & 0.00000 & 0.00000 & -1.16000 \\
 & & & 5.32000 & -0.70000 & 0.00000 \\
 & & & & 5.32000 & 0.00000 \\
 & & & & & 4.88000
\end{pmatrix}
\end{array}
$$

Depth of 1 km:

$$
\begin{array}{c}
 \\ 11 \\ 22 \\ 33 \\ 23 \\ 13 \\ 12
\end{array}
\begin{array}{c}
\begin{array}{cccccc} 11 & 22 & 33 & 23 & 13 & 12 \end{array} \\
\begin{pmatrix}
19.35852 & 5.34252 & 6.71500 & 0.00000 & 0.00000 & -3.53800 \\
 & 19.35852 & 6.71500 & 0.00000 & 0.00000 & -3.53800 \\
 & & 26.83100 & 0.00000 & 0.00000 & -1.76900 \\
 & & & 8.07552 & -1.06752 & 0.00000 \\
 & & & & 8.07552 & 0.00000 \\
 & & & & & 7.40452
\end{pmatrix}
\end{array}
$$

Coupling-ray-theory seismograms in models QIH and QI (transverse component)

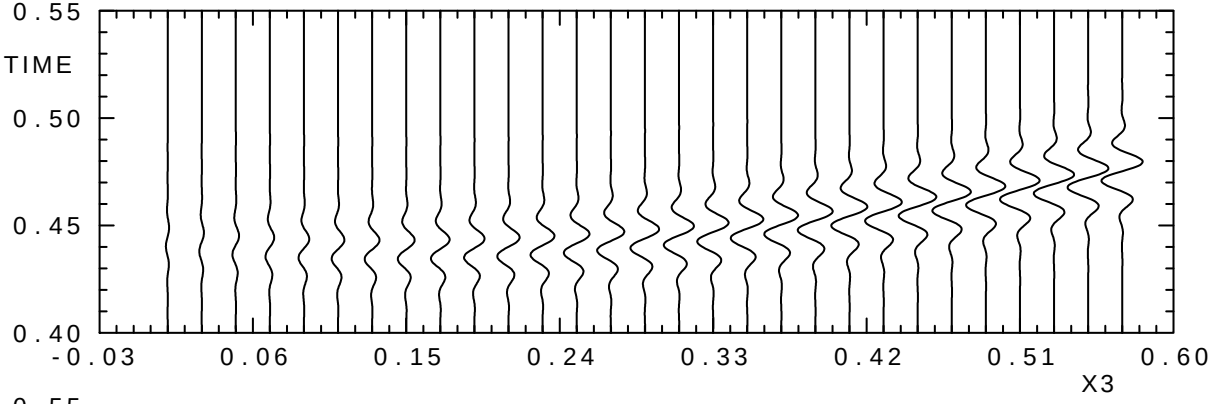

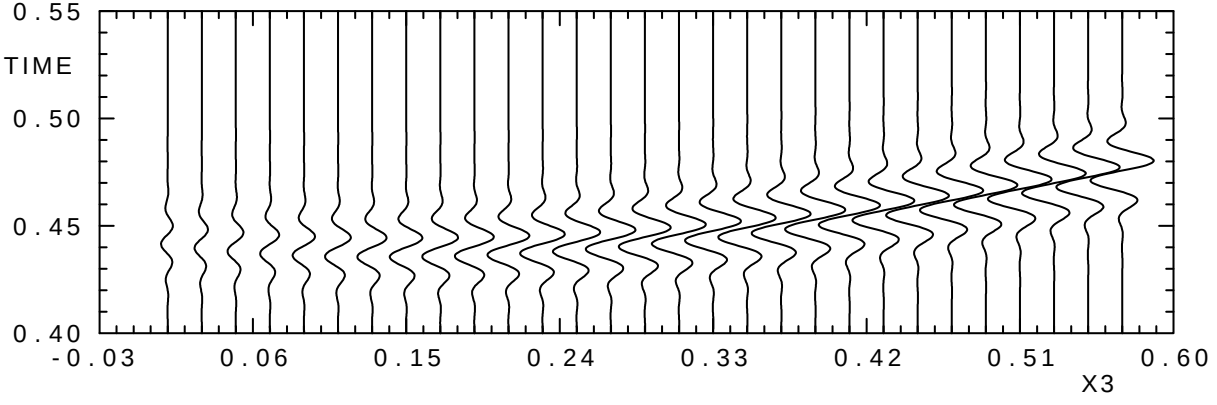

Coupling-ray-theory seismograms in models QI and QI2 (transverse component)

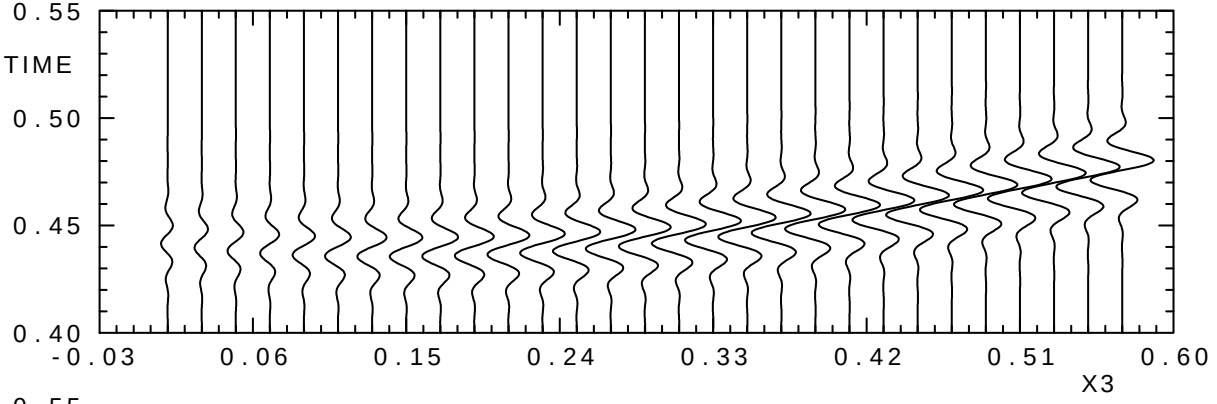

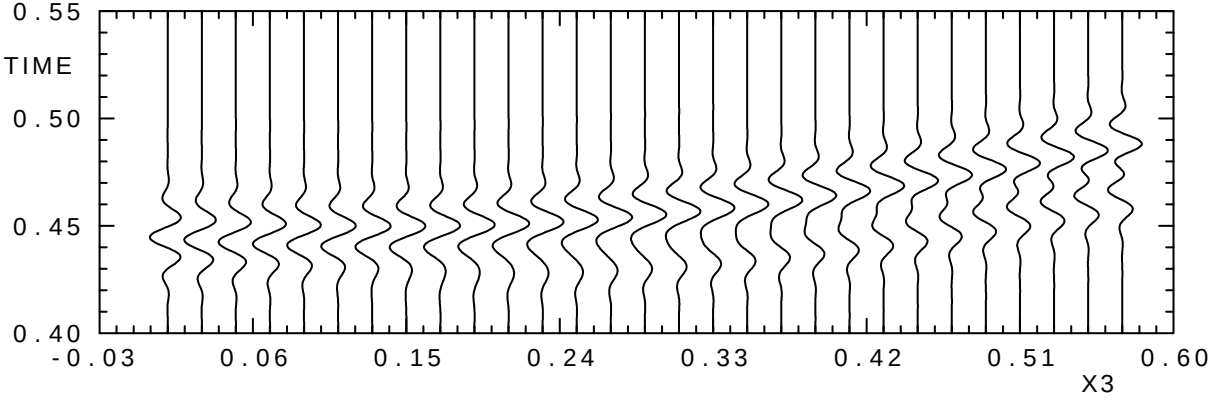

Coupling-ray-theory seismograms in models QI2 and QI4 (transverse component)

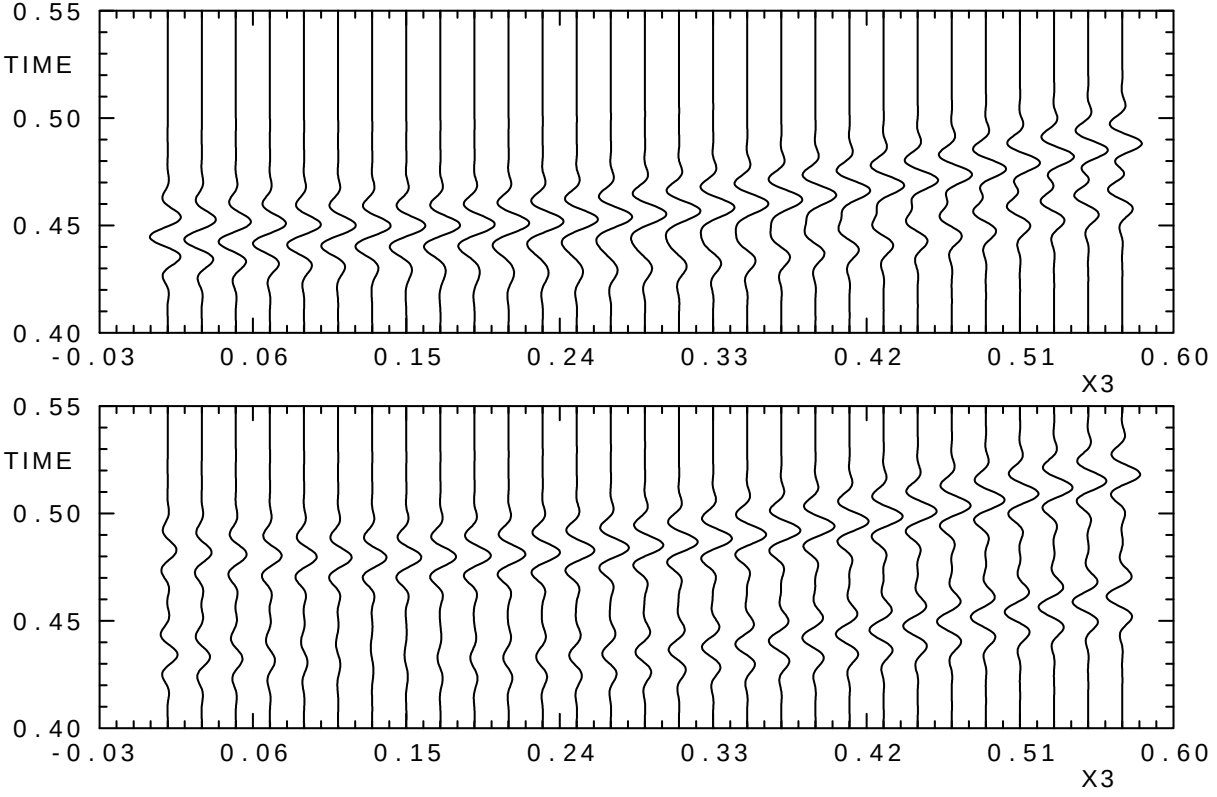

Outline

Introduction to the coupling ray theory for S waves

Prevailing-frequency approximation of the coupling ray theory

Reference rays for the coupling ray theory

Generally anisotropic medium which is approximately transversely isotropic

SH and SV reference rays in a generally anisotropic medium

Interpolation of the coupling-ray-theory Green function within ray cells

Conclusions

Idea of the prevailing-frequency approximation

Anisotropic-ray-theory Green function:

$$G_{ij}^{\mathrm{ART}}(\mathbf{x},\mathbf{x}_0,\omega) = \sum_{K=1}^{2} A^{(K)}(\mathbf{x},\mathbf{x}_0)\; g_i^{(K)}(\mathbf{x})\, g_j^{(K)}(\mathbf{x}_0)\; \exp[\mathrm{i}\omega\tau^{(K)}(\mathbf{x},\mathbf{x}_0)]$$

Coupling-ray-theory Green function:

$$G_{ij}^{\mathrm{CRT}}(\mathbf{x},\mathbf{x}_0,\omega)$$

Prevailing-frequency approximation
of the coupling-ray-theory Green function:

$$G_{ij}^{\mathrm{CRT}}(\mathbf{x},\mathbf{x}_0,\omega) \approx G_{ij}^{\mathrm{PFA}}(\mathbf{x},\mathbf{x}_0,\omega)$$

Prevailing-frequency Green function:

$$G_{ij}^{\mathrm{PFA}}(\mathbf{x},\mathbf{x}_0,\omega) = \sum_{K=1}^{2} A^{(K)}(\mathbf{x},\mathbf{x}_0)\, e_i^{(K)}(\mathbf{x},\omega_0)\, e_j^{(K)}(\mathbf{x}_0,\omega_0)\, \exp\big[\mathrm{i}\omega T^{(K)}(\mathbf{x},\mathbf{x}_0,\omega_0)\big]$$

ω_0... prevailing circular frequency.

$T^{(K)}(\mathbf{x},\mathbf{x}_0,\omega_0)$... coupling-ray-theory travel times.
$e_i^{(K)}(\mathbf{x},\omega_0)$, $e_j^{(K)}(\mathbf{x_0},\omega_0)$... coupling-ray-theory polarization vectors.

Prevailing-frequency Green function — conditions:

$$G_{ij}^{\mathrm{PFA}}(\mathbf{x}, \mathbf{x}_0, \omega_0) = G_{ij}^{\mathrm{CRT}}(\mathbf{x}, \mathbf{x}_0, \omega_0)$$

$$\frac{\partial G_{ij}^{\mathrm{PFA}}}{\partial \omega}(\mathbf{x}, \mathbf{x}_0, \omega_0) = \frac{\partial G_{ij}^{\mathrm{CRT}}}{\partial \omega}(\mathbf{x}, \mathbf{x}_0, \omega_0)$$

These conditions uniquely determine coupling-ray-theory travel times $T^{(K)}(\mathbf{x}, \mathbf{x}_0, \omega_0)$ and coupling-ray-theory polarization vectors $e_i^{(K)}(\mathbf{x}, \omega_0)$ and $e_j^{(K)}(\mathbf{x_0}, \omega_0)$.

We numerically calculate $G_{ij}^{\mathrm{CRT}}(\mathbf{x}, \mathbf{x}_0, \omega_0)$ using the algorithm by Bulant & Klimeš (2002).

We calculate $\frac{\partial G_{ij}^{\mathrm{CRT}}}{\partial \omega}(\mathbf{x}, \mathbf{x}_0, \omega_0)$ using the derivative of this algorithm.

Numerical comparison of seismograms

Prevailing-frequency approximation.
Standard coupling ray theory.
Fourier pseudospectral method.

Source-receiver configuration:

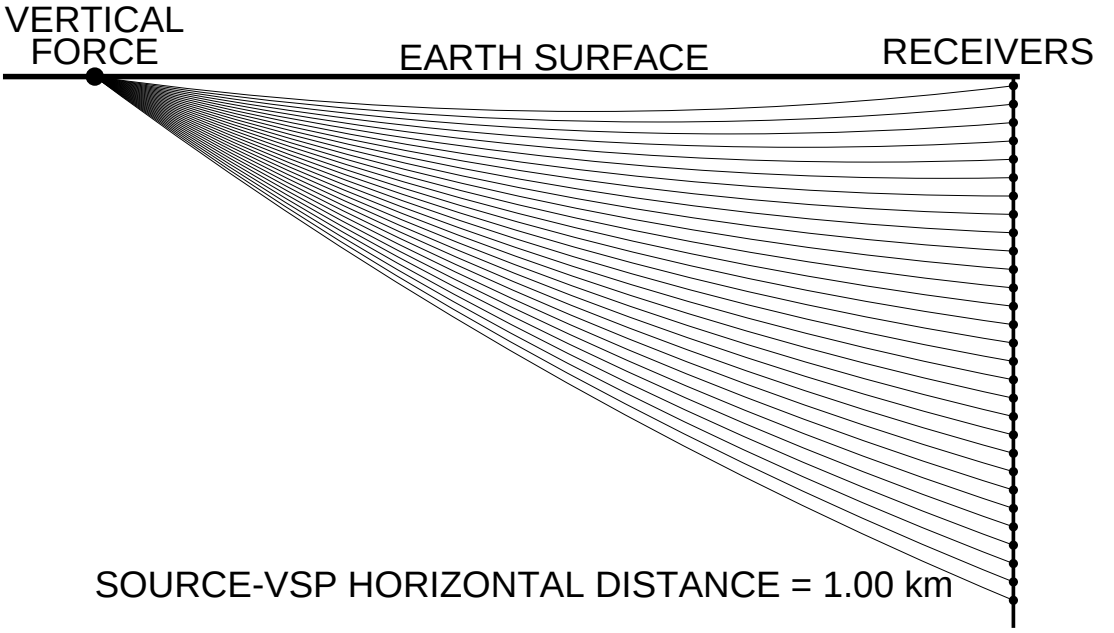

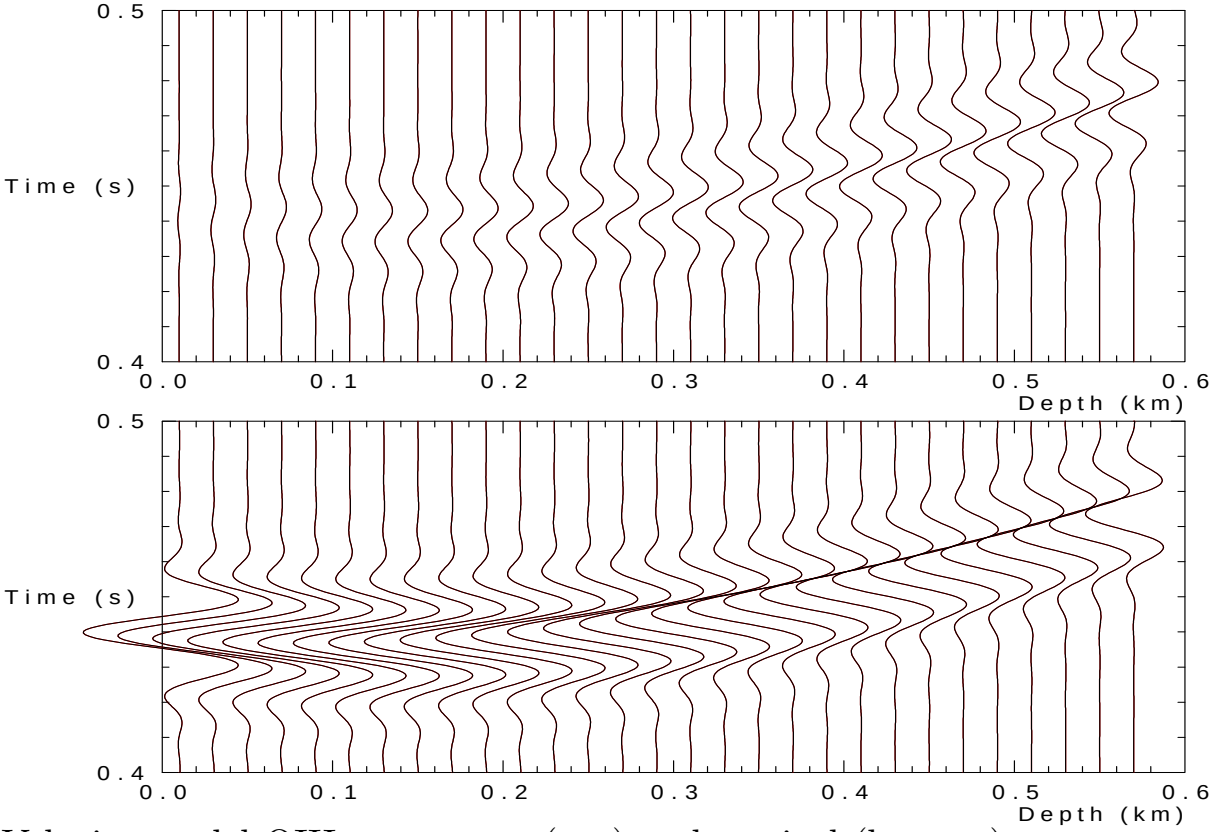

Velocity model QIH, transverse (top) and vertical (bottom) component. Prevailing-frequency approximation, standard coupling ray theory.

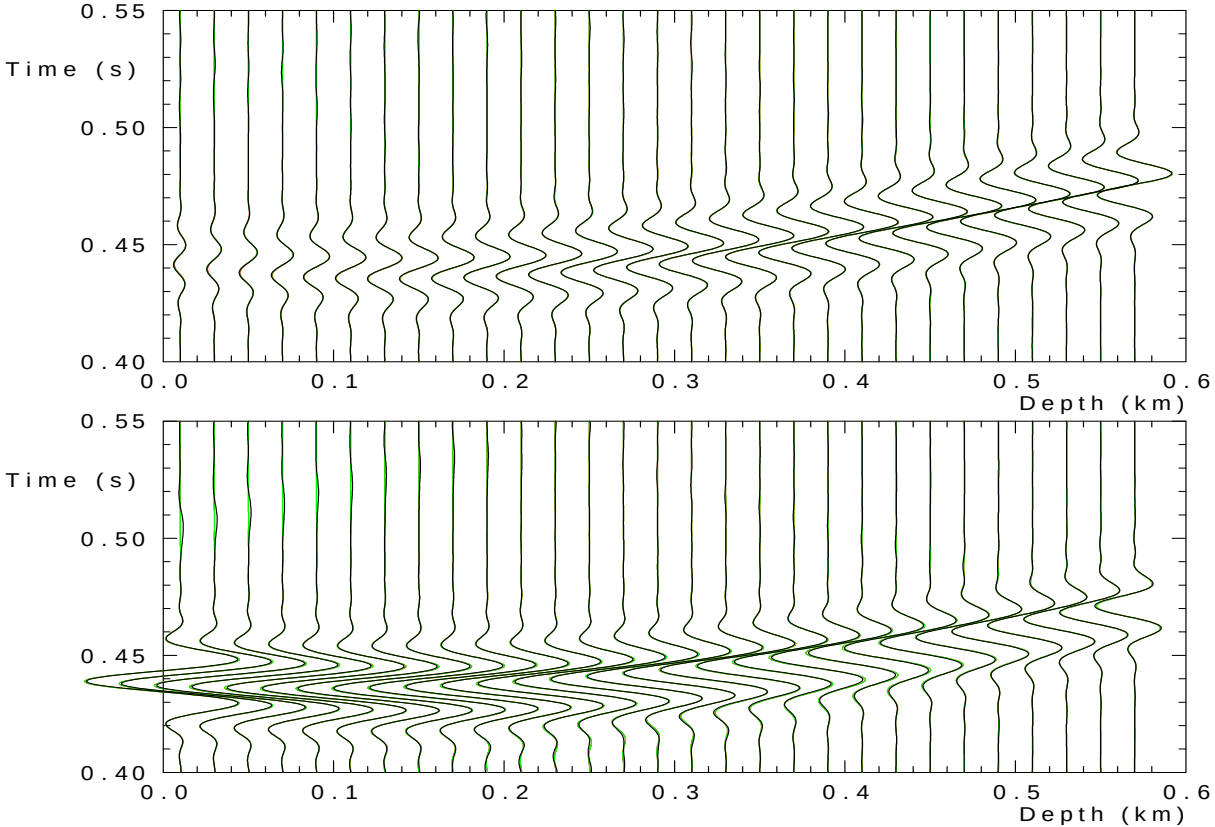

Velocity model QI, transverse (top) and vertical (bottom) component. Prevailing-frequency, coupling ray theory, Fourier pseudospectral method.

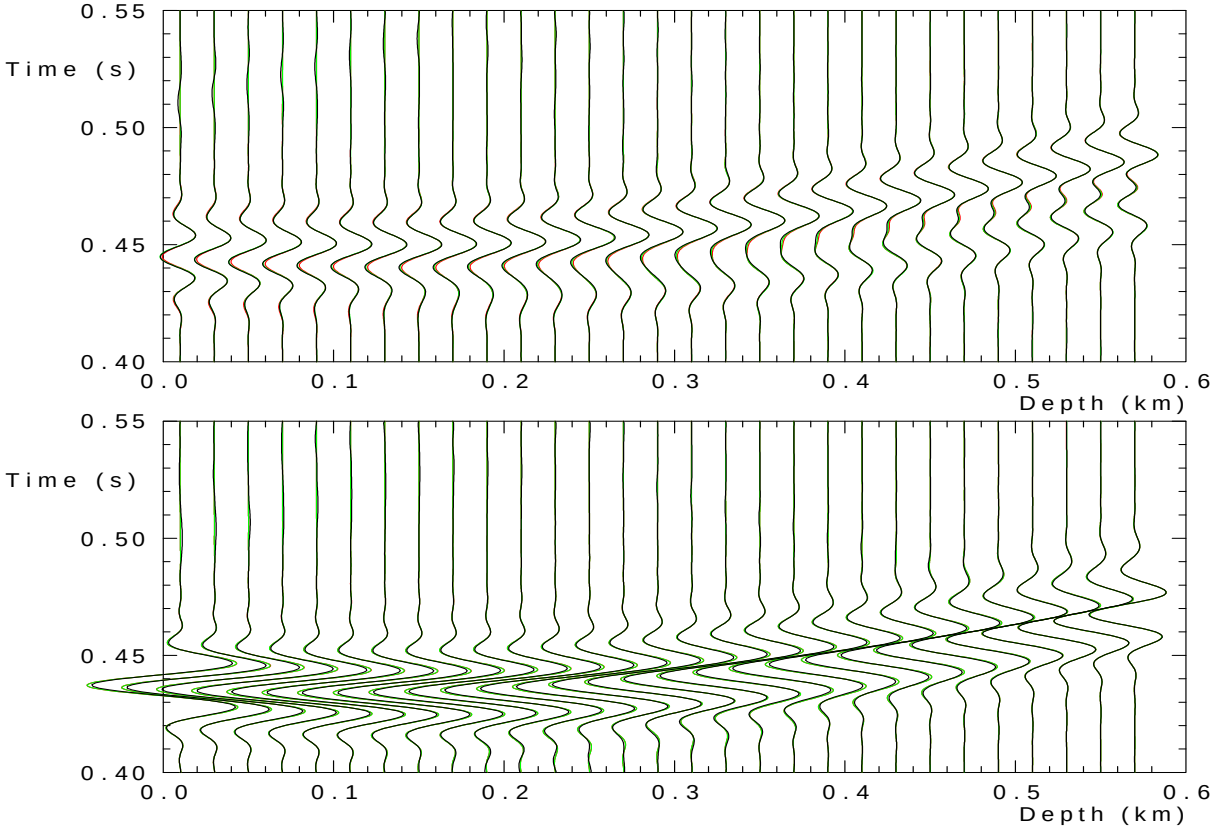

Velocity model QI2, transverse (top) and vertical (bottom) component. Prevailing-frequency, coupling ray theory, Fourier pseudospectral method.

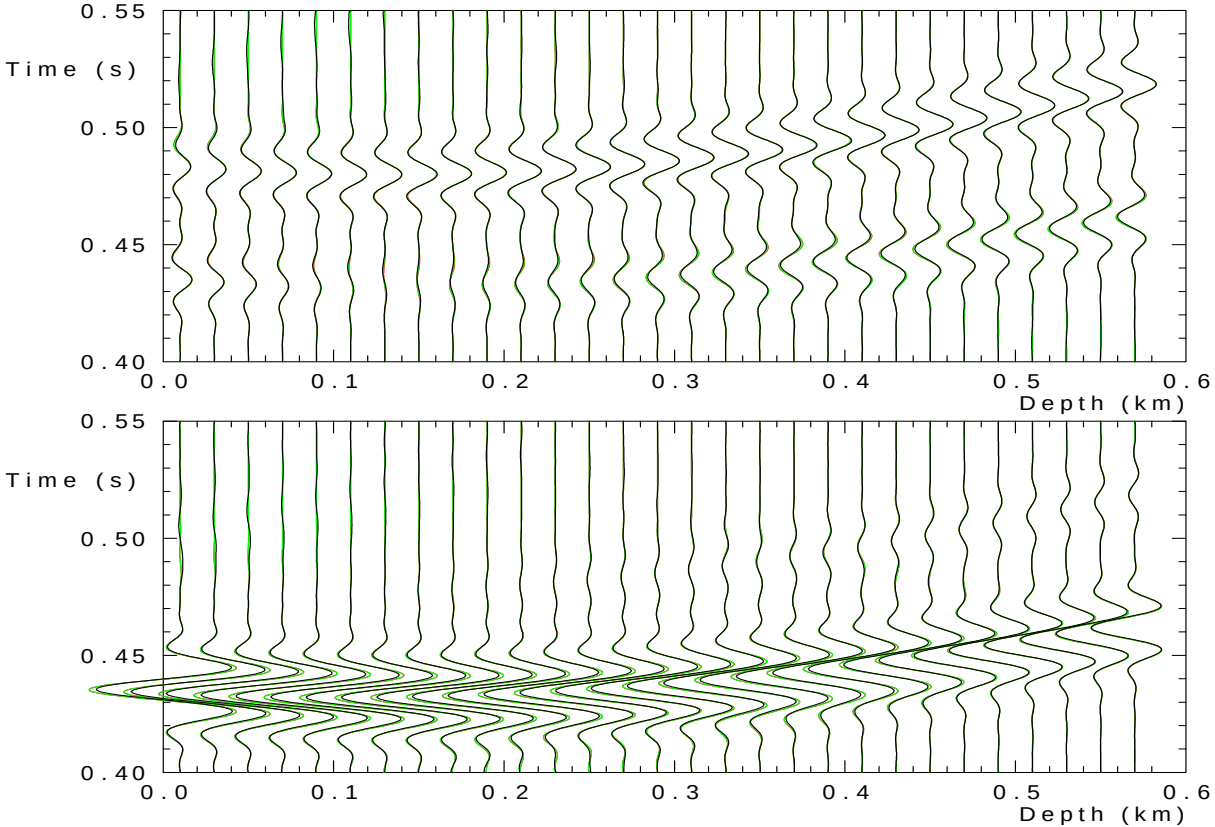

Velocity model QI4, transverse (top) and vertical (bottom) component. Prevailing-frequency, coupling ray theory, Fourier pseudospectral method.

Density-normalized stiffness tensor in velocity model KISS

Depth of 0 km:

$$
\begin{array}{c}
 \\ 11 \\ 22 \\ 33 \\ 23 \\ 13 \\ 12
\end{array}
\begin{array}{c}
\begin{array}{cccccc} 11 & 22 & 33 & 23 & 13 & 12 \end{array} \\
\begin{pmatrix}
13.39063 & 4.46008 & 4.46018 & 0.00000 & 0.00000 & -0.01797 \\
 & 15.70921 & 5.03982 & 0.00000 & 0.00000 & -0.02251 \\
 & & 15.71000 & 0.00000 & 0.00000 & -0.01012 \\
 & & & 5.32989 & -0.00611 & 0.00000 \\
 & & & & 4.98011 & 0.00000 \\
 & & & & & 4.98008
\end{pmatrix}
\end{array}
$$

Depth of 1 km:

$$
\begin{array}{c}
 \\ 11 \\ 22 \\ 33 \\ 23 \\ 13 \\ 12
\end{array}
\begin{array}{c}
\begin{array}{cccccc} 11 & 22 & 33 & 23 & 13 & 12 \end{array} \\
\begin{pmatrix}
20.42072 & 6.80162 & 6.80177 & 0.00000 & 0.00000 & -0.02741 \\
 & 23.95656 & 7.68573 & 0.00000 & 0.00000 & -0.03433 \\
 & & 23.95775 & 0.00000 & 0.00000 & -0.01543 \\
 & & & 8.12810 & -0.00931 & 0.00000 \\
 & & & & 7.59466 & 0.00000 \\
 & & & & & 7.59462
\end{pmatrix}
\end{array}
$$

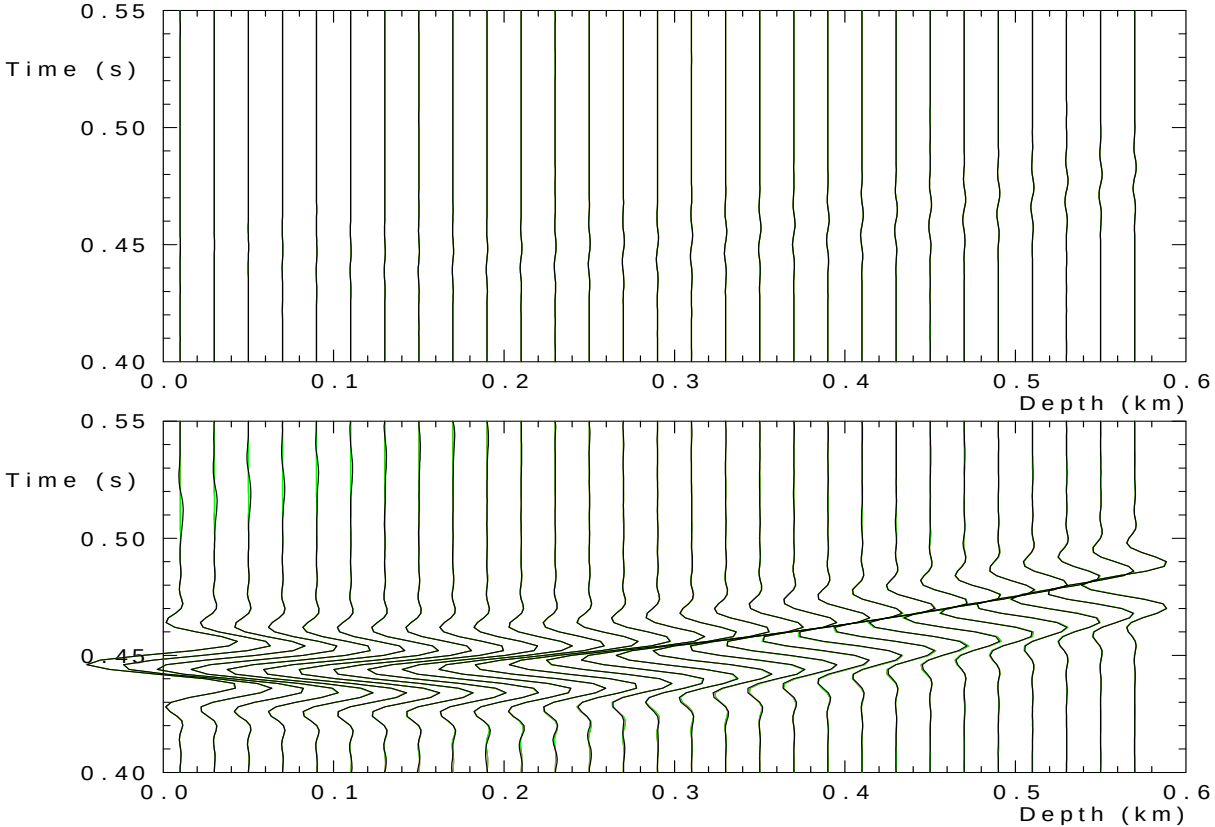

Velocity model KISS, transverse (top) and vertical (bottom) component.
Prevailing-frequency, coupling ray theory, Fourier pseudospectral method.

Density-normalized stiffness tensor in velocity model SC1_I

Depth of 0 km:

$$
\begin{array}{c}
 \\ 11 \\ 22 \\ 33 \\ 23 \\ 13 \\ 12
\end{array}
\begin{array}{c}
\begin{array}{cccccc} 11 & 22 & 33 & 23 & 13 & 12 \end{array} \\
\begin{pmatrix}
19.14000 & 8.35500 & 7.42250 & 0.00000 & 0.00000 & 0.50663 \\
 & 19.23000 & 7.44750 & 0.00000 & 0.00000 & -0.58457 \\
 & & 20.22000 & 0.00000 & 0.00000 & -0.02165 \\
 & & & 6.06000 & -0.55426 & 0.00000 \\
 & & & & 5.42000 & 0.00000 \\
 & & & & & 6.04500
\end{pmatrix}
\end{array}
$$

Depth of 1.5 km:

$$
\begin{array}{c}
 \\ 11 \\ 22 \\ 33 \\ 23 \\ 13 \\ 12
\end{array}
\begin{array}{c}
\begin{array}{cccccc} 11 & 22 & 33 & 23 & 13 & 12 \end{array} \\
\begin{pmatrix}
30.25 & 10.08 & 10.08 & 0.00 & 0.00 & 0.00 \\
 & 30.25 & 10.08 & 0.00 & 0.00 & 0.00 \\
 & & 30.25 & 0.00 & 0.00 & 0.00 \\
 & & & 10.08 & 0.00 & 0.00 \\
 & & & & 10.08 & 0.00 \\
 & & & & & 10.08
\end{pmatrix}
\end{array}
$$

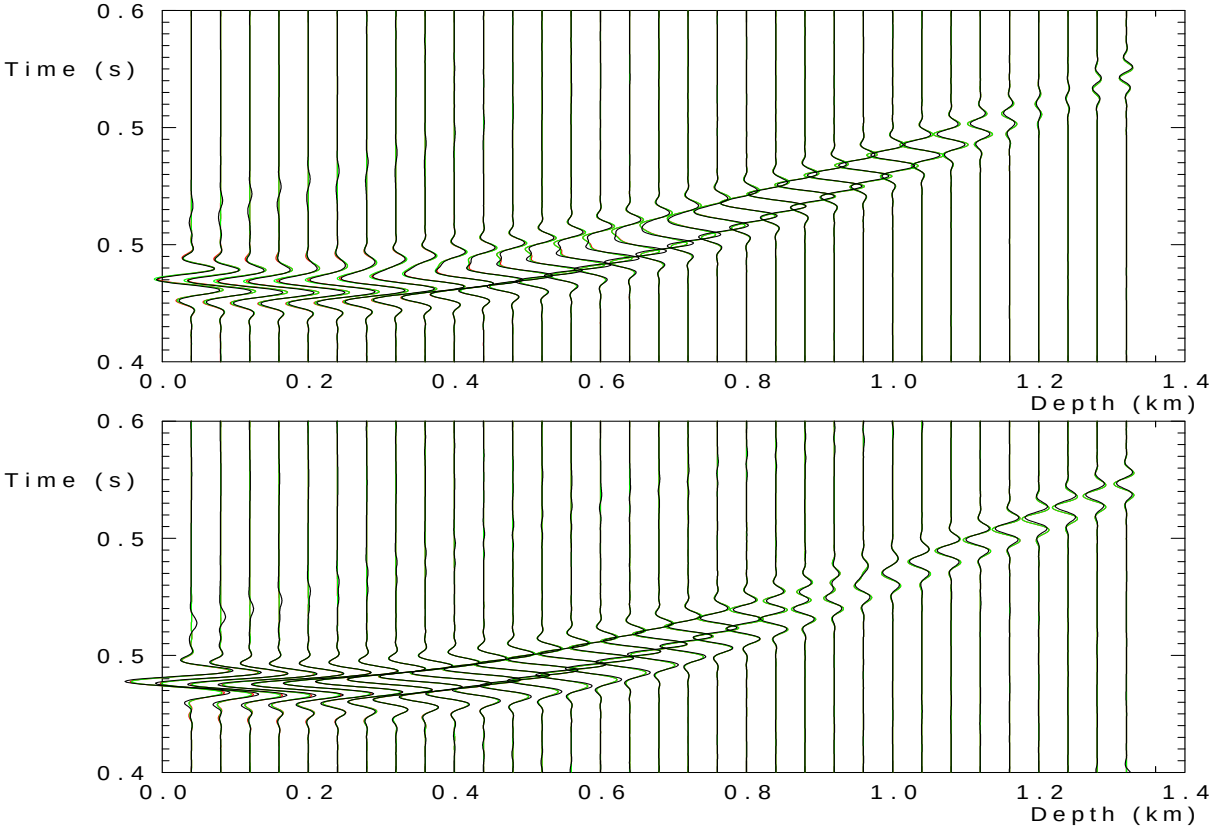

Velocity model SC1_I, transverse (top) and vertical (bottom) component.
Prevailing-frequency, coupling ray theory, Fourier pseudospectral method.

Density-normalized stiffness tensor in velocity model SC1_II

Depth of 0 km:

$$
\begin{array}{c}
 \\ 11 \\ 22 \\ 33 \\ 23 \\ 13 \\ 12
\end{array}
\begin{array}{c}
\begin{array}{cccccc} 11 & 22 & 33 & 23 & 13 & 12 \end{array} \\
\begin{pmatrix}
18.97125 & 7.67125 & 8.36125 & 0.46000 & -0.31177 & -0.15589 \\
 & 19.64625 & 7.74375 & -0.49500 & 0.25115 & -0.42868 \\
 & & 18.87000 & -0.02250 & -0.03897 & 0.53477 \\
 & & & 5.89500 & 0.26847 & -0.28146 \\
 & & & & 6.20500 & 0.15250 \\
 & & & & & 5.97625
\end{pmatrix}
\end{array}
$$

Depth of 1.5 km:

$$
\begin{array}{c}
 \\ 11 \\ 22 \\ 33 \\ 23 \\ 13 \\ 12
\end{array}
\begin{array}{c}
\begin{array}{cccccc} 11 & 22 & 33 & 23 & 13 & 12 \end{array} \\
\begin{pmatrix}
30.25 & 10.08 & 10.08 & 0.00 & 0.00 & 0.00 \\
 & 30.25 & 10.08 & 0.00 & 0.00 & 0.00 \\
 & & 30.25 & 0.00 & 0.00 & 0.00 \\
 & & & 10.08 & 0.00 & 0.00 \\
 & & & & 10.08 & 0.00 \\
 & & & & & 10.08
\end{pmatrix}
\end{array}
$$

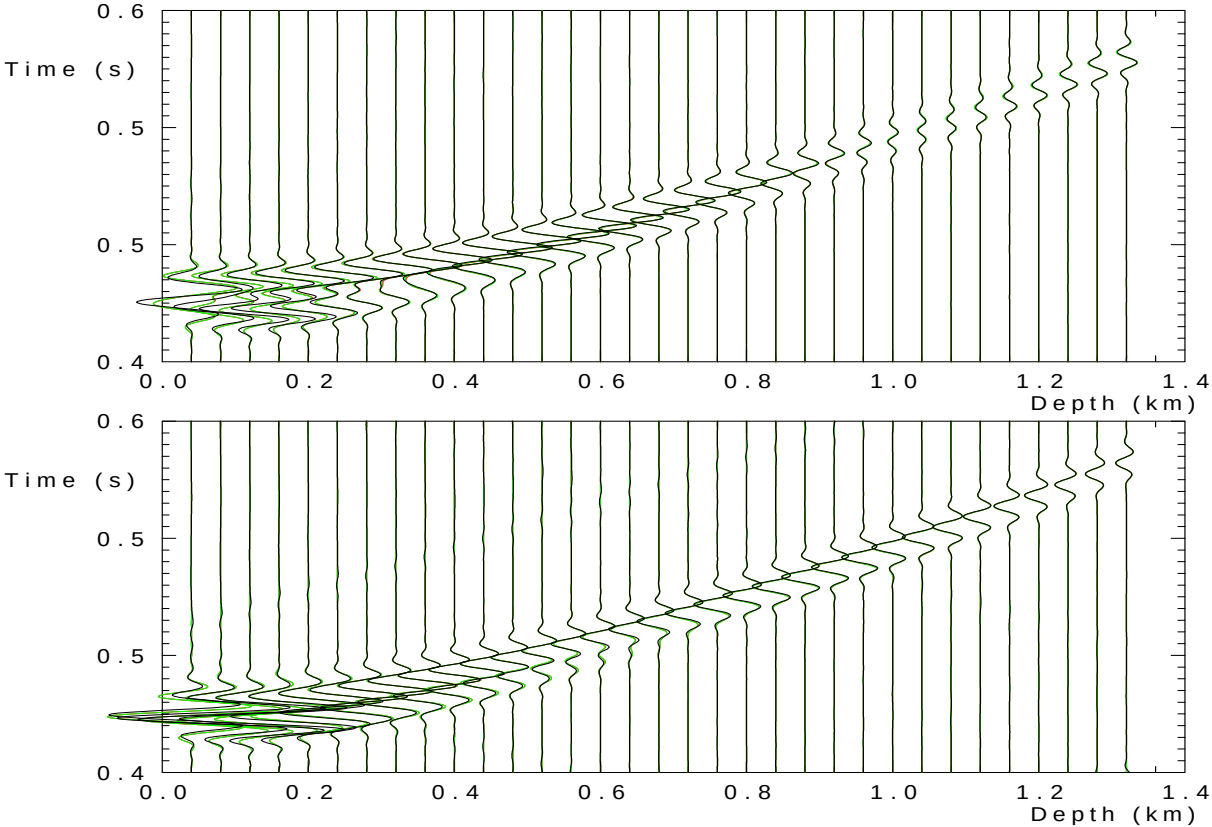

Velocity model SC1_II, transverse (top) & vertical (bottom) component.
Prevailing-frequency, coupling ray theory, Fourier pseudospectral method.

Density-normalized stiffness tensor in velocity model ORT

Depth of 0 km:

$$
\begin{array}{c}
 \\ 11 \\ 22 \\ 33 \\ 23 \\ 13 \\ 12
\end{array}
\begin{array}{c}
\begin{array}{cccccc} 11 & 22 & 33 & 23 & 13 & 12 \end{array} \\
\begin{pmatrix}
8.16473 & 4.23111 & 3.72962 & 0.00000 & 0.00000 & -0.03645 \\
 & 8.18304 & 3.73288 & 0.00000 & 0.00000 & -0.06815 \\
 & & 7.48000 & 0.00000 & 0.00000 & -0.01868 \\
 & & & 1.87936 & -0.04981 & 0.00000 \\
 & & & & 1.87064 & 0.00000 \\
 & & & & & 2.15111
\end{pmatrix}
\end{array}
$$

Depth of 3 km:

$$
\begin{array}{c}
 \\ 11 \\ 22 \\ 33 \\ 23 \\ 13 \\ 12
\end{array}
\begin{array}{c}
\begin{array}{cccccc} 11 & 22 & 33 & 23 & 13 & 12 \end{array} \\
\begin{pmatrix}
17.88851 & 9.27758 & 8.17515 & 0.00000 & 0.00000 & -0.08040 \\
 & 17.92882 & 8.18234 & 0.00000 & 0.00000 & -0.14997 \\
 & & 16.39250 & 0.00000 & 0.00000 & -0.04109 \\
 & & & 4.11209 & -0.10958 & 0.00000 \\
 & & & & 4.09291 & 0.00000 \\
 & & & & & 4.71008
\end{pmatrix}
\end{array}
$$

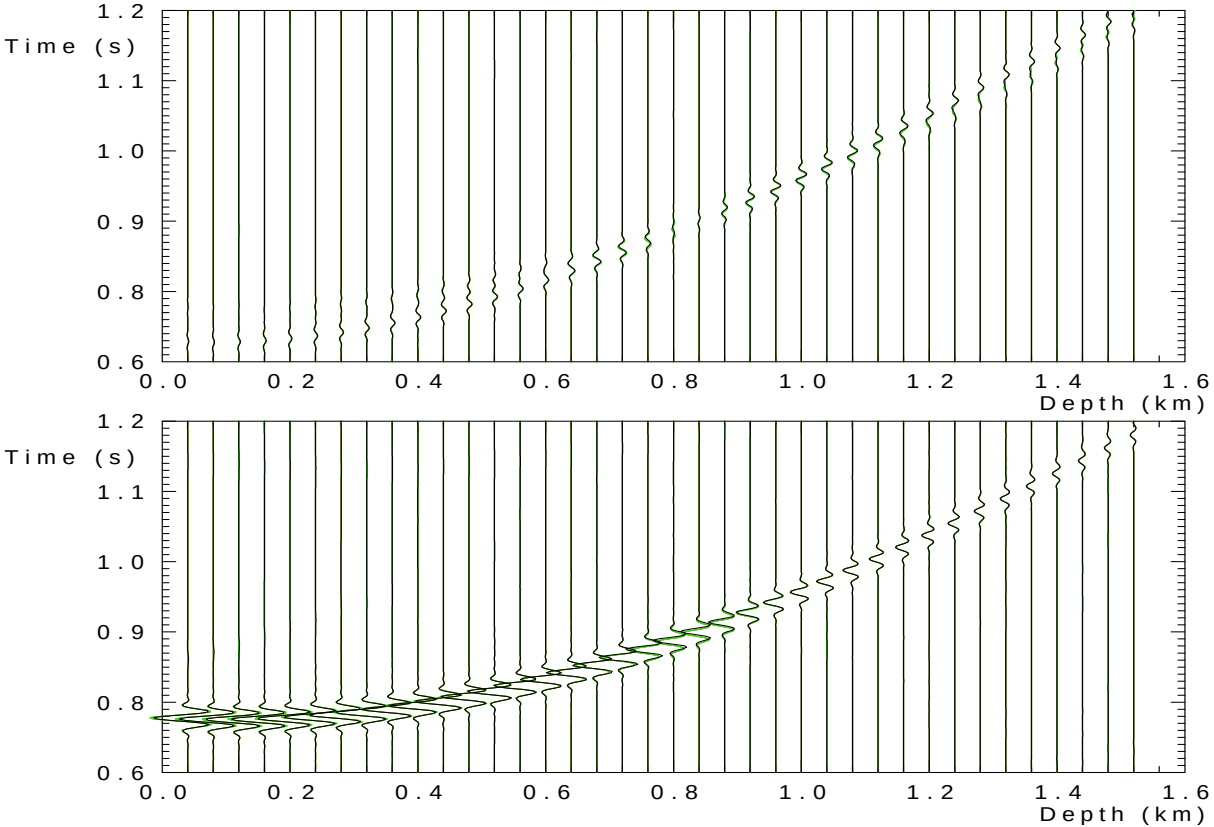

Velocity model ORT, transverse (top) and vertical (bottom) component.
Prevailing-frequency, coupling ray theory, Fourier pseudospectral method.

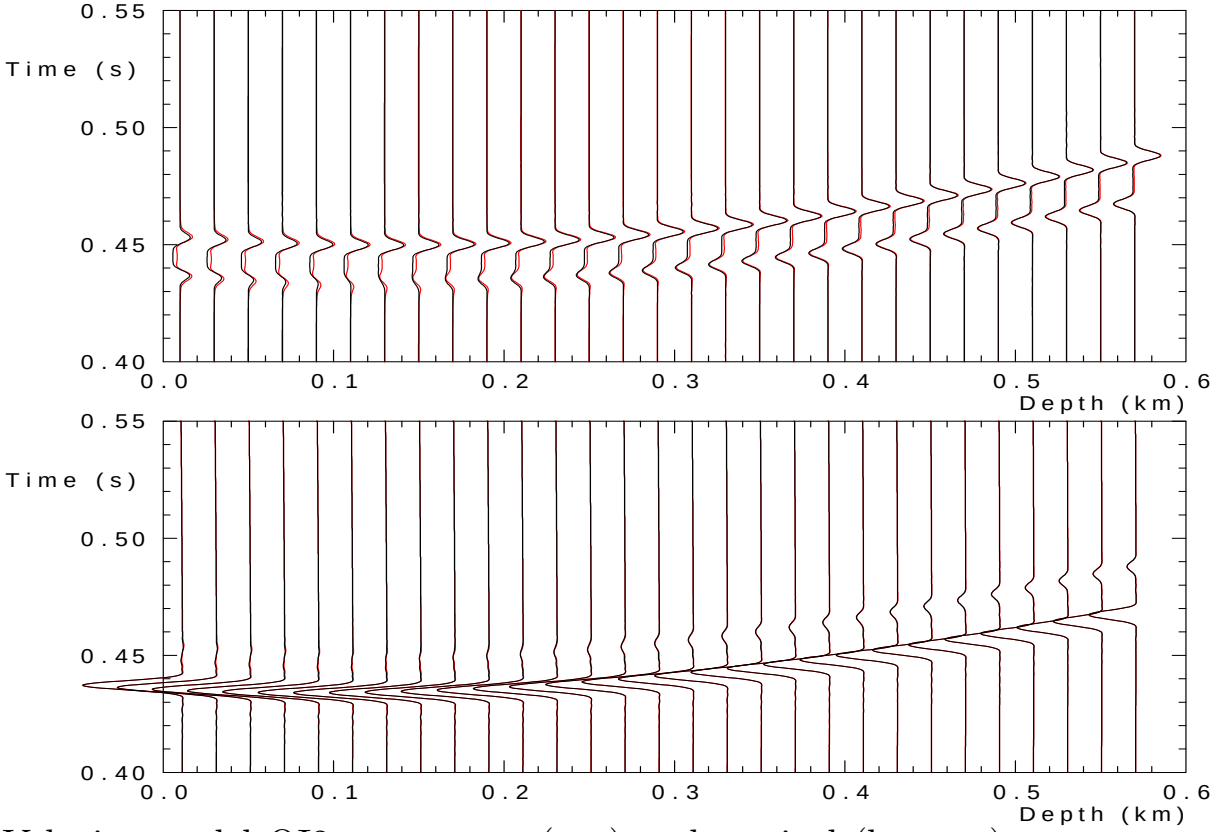

Velocity model QI2, transverse (top) and vertical (bottom) component. Broad-band 3 Hz–80 Hz. Prevailing-frequency, coupling ray theory.

Outline

Introduction to the coupling ray theory for S waves

Prevailing-frequency approximation of the coupling ray theory

Reference rays for the coupling ray theory

Generally anisotropic medium which is approximately transversely isotropic

SH and SV reference rays in a generally anisotropic medium

Interpolation of the coupling-ray-theory Green function within ray cells

Conclusions

Reference rays for the coupling ray theory

Isotropic common reference rays

Traced in the isotropic reference velocity model.
Least accurate.

Anisotropic common reference rays

Traced using the averaged Hamiltonian function of both anisotropic-ray-theory S waves.
Universal option.
Always better than the isotropic common reference rays.

Anisotropic-ray-theory rays

Usually unusable.
Brief demonstration will follow.

SH and SV reference rays

Very accurate in generally anisotropic velocity models with considerable transversely isotropic components.
Demonstration of accuracy will follow.

Examples of singularities at the slowness surface

Along the reference ray, the slowness vector smoothly rotates according to Hamilton's equations of rays, and thus moves along the slowness surface.

Let us see how the slowness vector moves along the slowness surface.

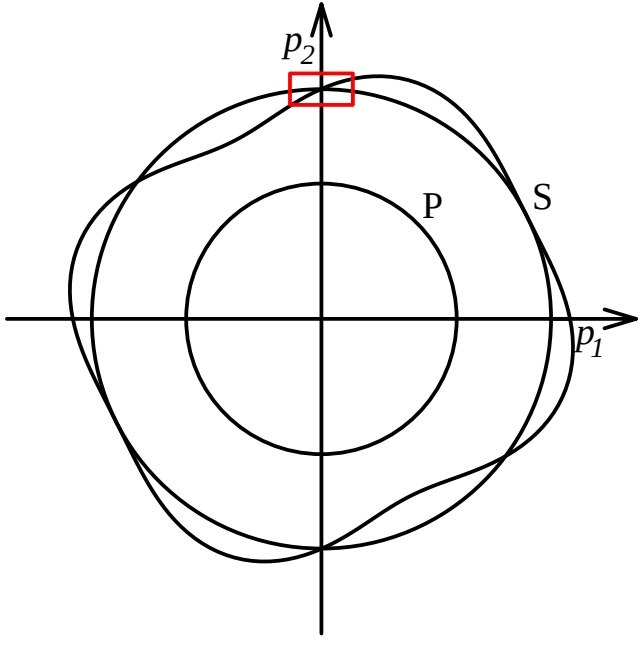

INTERSECTION SINGULARITY AT THE SLOWNESS SURFACE

SPLIT INTERSECTION SINGULARITY AT THE SLOWNESS SURFACE

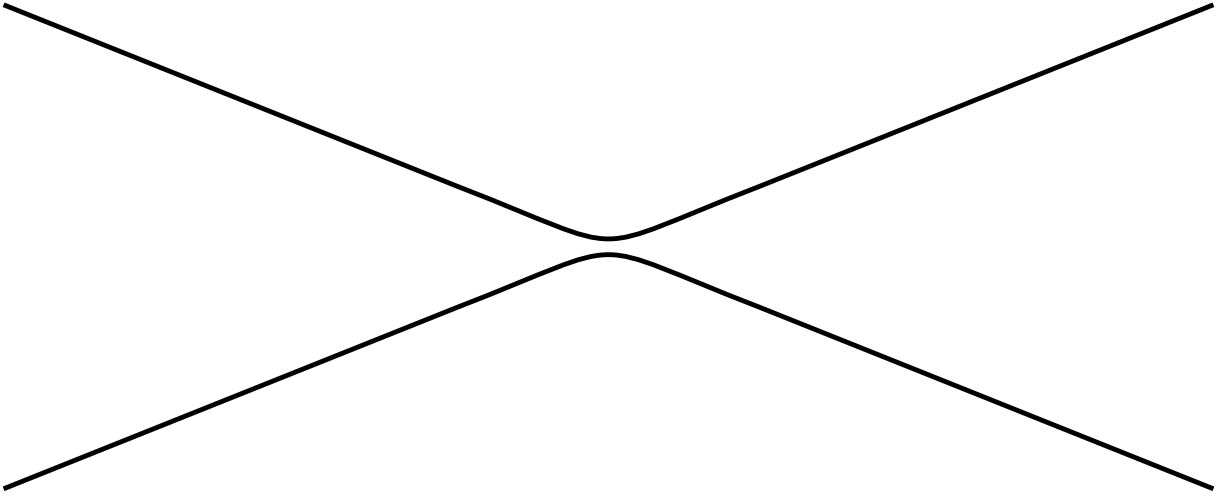

SPLIT INTERSECTION SINGULARITY AT THE SLOWNESS SURFACE

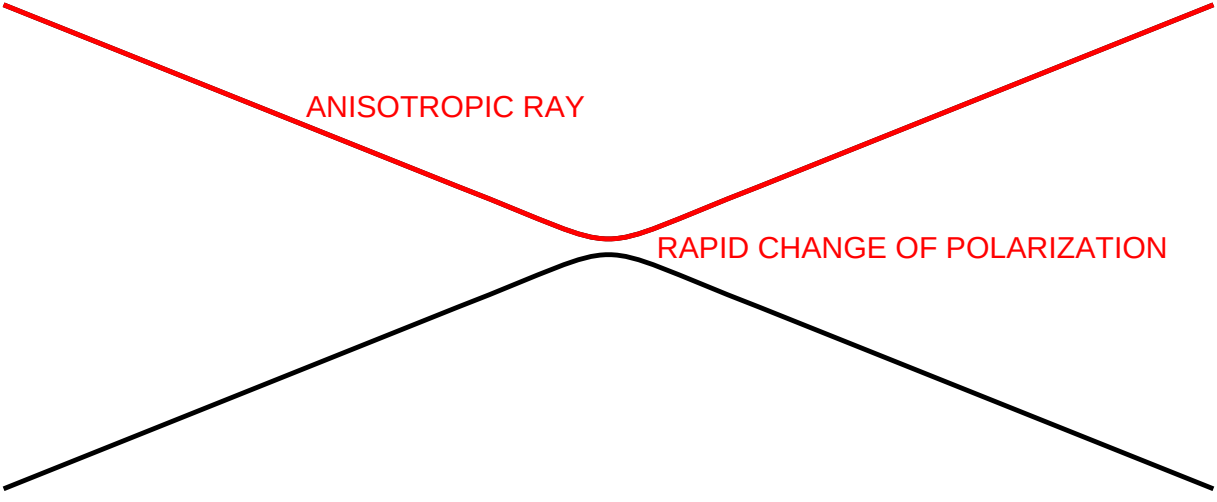

SPLIT INTERSECTION SINGULARITY AT THE SLOWNESS SURFACE

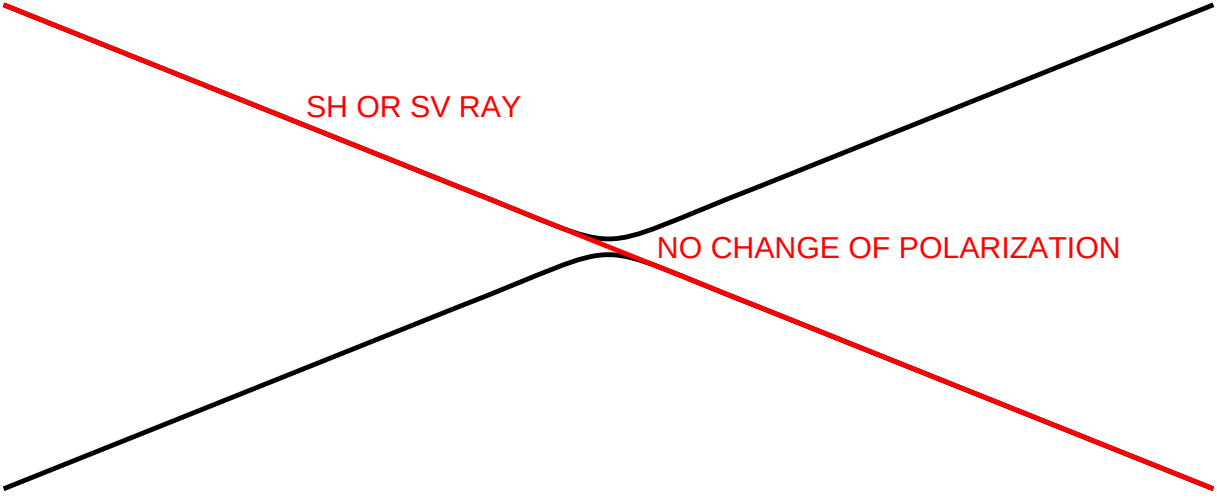

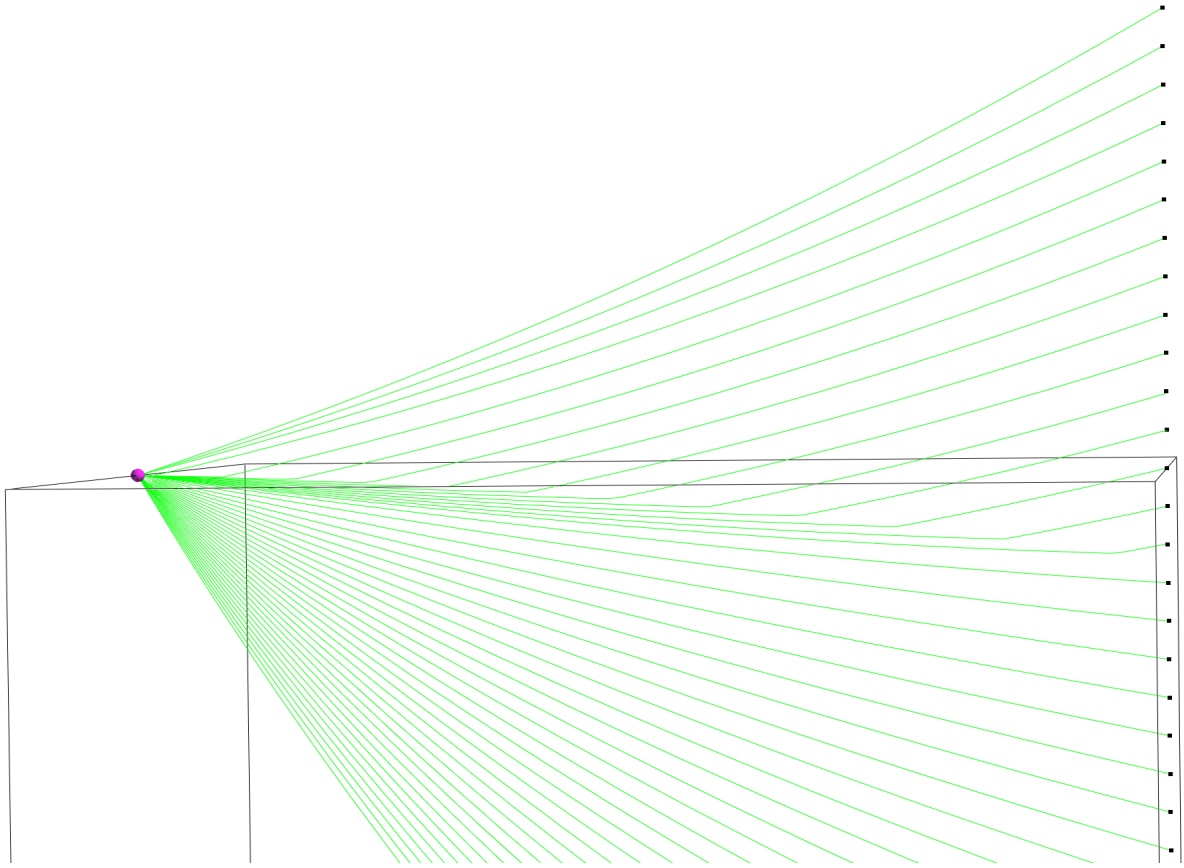

Anisotropic-ray-theory rays of the faster S wave in velocity model SC1_II.

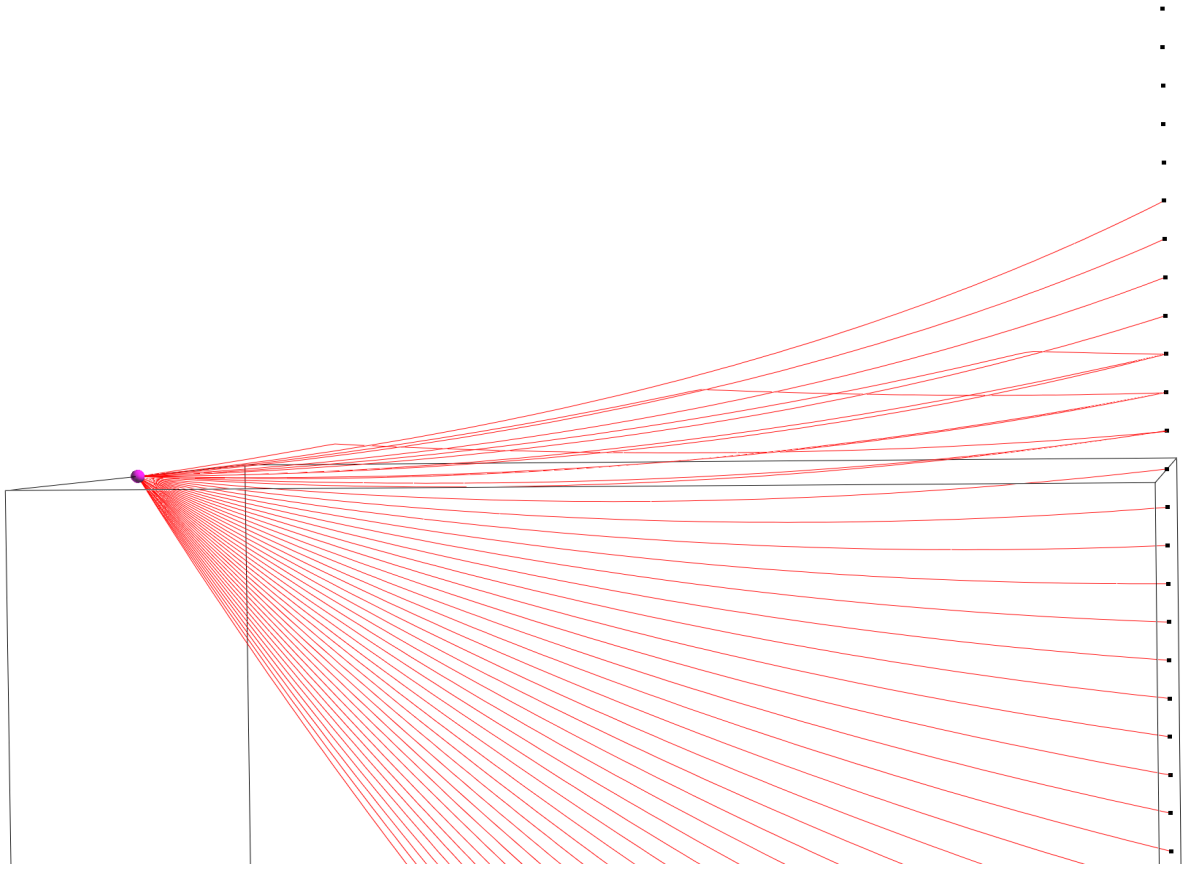

Anisotropic-ray-theory rays of the slower S wave in velocity model SC1_II.

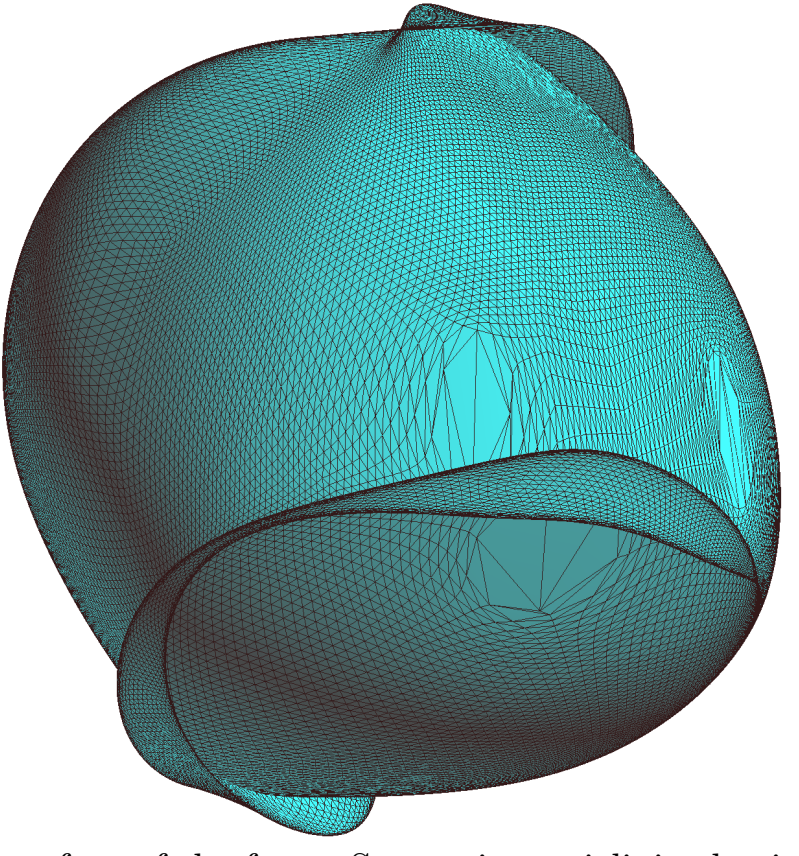

Ray-velocity surface of the faster S wave in a triclinic elastic medium.

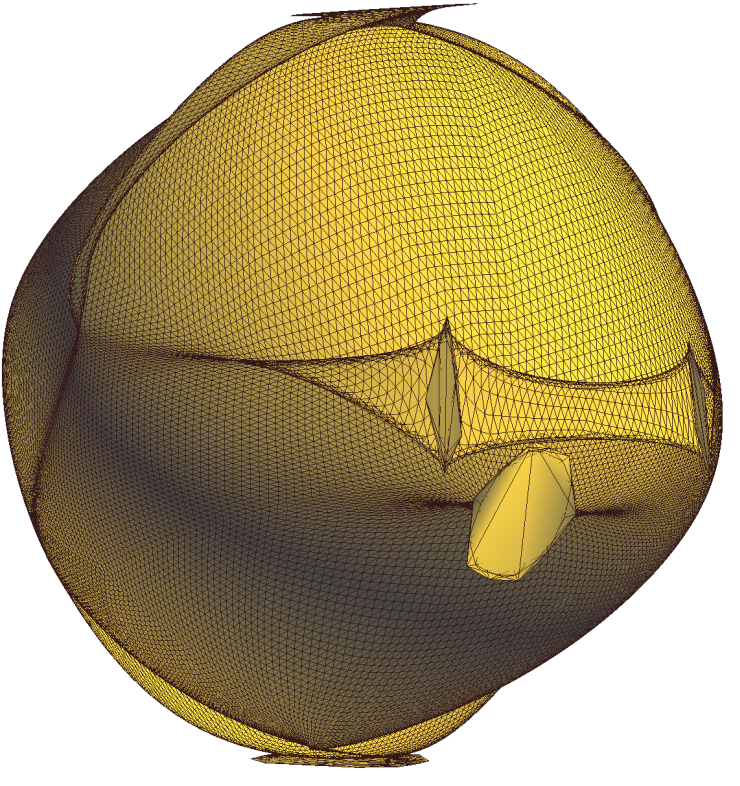

Ray-velocity surface of the slower S wave in a triclinic elastic medium.

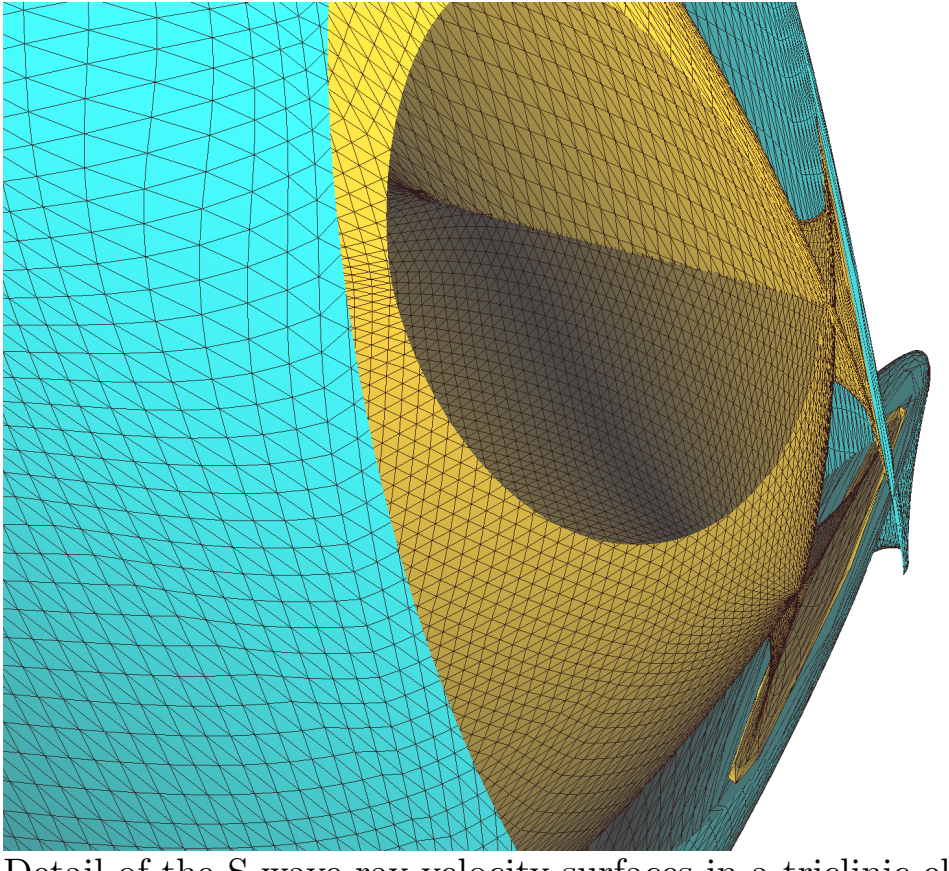

Detail of the S-wave ray-velocity surfaces in a triclinic elastic medium.

Outline

Introduction to the coupling ray theory for S waves

Prevailing-frequency approximation of the coupling ray theory

Reference rays for the coupling ray theory

Generally anisotropic medium which is approximately transversely isotropic

SH and SV reference rays in a generally anisotropic medium

Interpolation of the coupling-ray-theory Green function within ray cells

Conclusions

Determination of the reference symmetry axis of a generally anisotropic medium which is approximately transversely isotropic (Klimeš, 2015)

For a given stiffness tensor (tensor of elastic moduli) a_{ijkl} of a generally anisotropic medium, we estimate to which extent is the medium transversely isotropic and determine the direction of its reference symmetry axis in terms of the reference symmetry vector.

We consider the rotation $a_{ijkl}(\varphi)$ of stiffness tensor $a_{ijkl} = a_{ijkl}(0)$ about given unit vector t_i by angle φ. The derivative of the stiffness tensor with respect to the angle φ of rotation is

$$a'_{ijkl} = \frac{\mathrm{d}a_{ijkl}}{\mathrm{d}\varphi}(0) \quad .$$

We choose the square

$$y = a'_{ijkl}\, a'_{ijkl}$$

of the norm of the derivative of the stiffness tensor with respect to the angle of rotation as the objective function.

The objective function can be expressed as the quadratic form

$$y = t_m B_{mn} t_n$$

with positive-semidefinite 3×3 matrix B_{mn}. We denote the eigenvalues of matrix B_{mn} from the greatest to the smallest by $B_{(1)}$, $B_{(2)}$ and $B_{(3)}$, and the corresponding unit eigenvectors by $t_{i(1)}$, $t_{i(2)}$ and $t_{i(3)}$.

The reference symmetry vector is $t_{i(3)}$.
The non-TI ratio $\rho_{(3)} = \sqrt{B_{(3)}}/\sqrt{a_{ijkl}\, a_{ijkl}}$ characterizes the extent to which the medium is not transversely isotropic.

Outline

Introduction to the coupling ray theory for S waves

Prevailing-frequency approximation of the coupling ray theory

Reference rays for the coupling ray theory

Generally anisotropic medium which is approximately transversely isotropic

SH and SV reference rays in a generally anisotropic medium

Interpolation of the coupling-ray-theory Green function within ray cells

Conclusions

SH and SV reference rays in generally anisotropic media (Klimeš & Bulant, 2015)

The reference symmetry axis is determined by given reference symmetry vector t_i.

We project reference symmetry vector t_i onto the plane defined by two S-wave eigenvectors $g_{i(1)}$ and $g_{i(2)}$ of Christoffel matrix Γ_{jk}, corresponding to eigenvalues $G_{(1)}$ and $G_{(2)}$. We define the unit reference SV polarization vector in the direction of this projection (Einstein summation):

$$g_{i\mathrm{SV}} = \frac{g_{i(A)}\, g_{k(A)}\, t_k}{\sqrt{t_r\, g_{r(N)}\, g_{s(N)}\, t_s}} \quad , \qquad A, N = 1, 2 \quad .$$

We define the reference SV Hamiltonian function as

$$H_{\mathrm{SV}} = \tfrac{1}{2}\, g_{j\mathrm{SV}}\, \Gamma_{jk}\, g_{k\mathrm{SV}} \quad .$$

We then define the reference SH Hamiltonian function as

$$H_{\mathrm{SH}} = \tfrac{1}{2}\left(G_{(1)} + G_{(2)}\right) - H_{\mathrm{SV}} \quad .$$

We calculate the first-order and second-order phase-space derivatives of the reference SV and SH Hamiltonian functions (Klimeš & Bulant, 2015) and trace the SV and SH reference rays.

Coupling ray theory along the SH and SV reference rays

In a generally anisotropic velocity model with a considerable transversely isotropic component (Klimeš, 2015), we trace the SH and SV reference rays according to Klimeš & Bulant (2015).

We apply the prevailing-frequency approximation of the coupling ray theory to the SH and SV reference rays.

We obtain two S-wave arrivals along each SH ray and have to select the right one of them. Analogously, we obtain two S-wave arrivals along each SV ray and have to select the right one of them. We select the right arrivals according to their polarization and travel time (Klimeš & Bulant, 2014a).

Accuracy of the synthetic seismograms calculated along the SH and SV reference rays

The **red** seismograms are calculated using the prevailing-frequency approximation of the coupling ray theory
(a) along the anisotropic common S-wave reference rays with the quadratic perturbation expansions of travel times, and
(b) along the SH and SV reference rays with the linear perturbation expansions of travel times.

They are overlaid by the **black** seismograms calculated using the Fourier pseudospectral method by Pšenčík, Farra & Tessmer (2012) which is considered here as a nearly exact reference.

Numerical comparison of seismograms in velocity models QI2 and QI4 (Klimeš & Bulant, 2014a)

Source-receiver configuration:

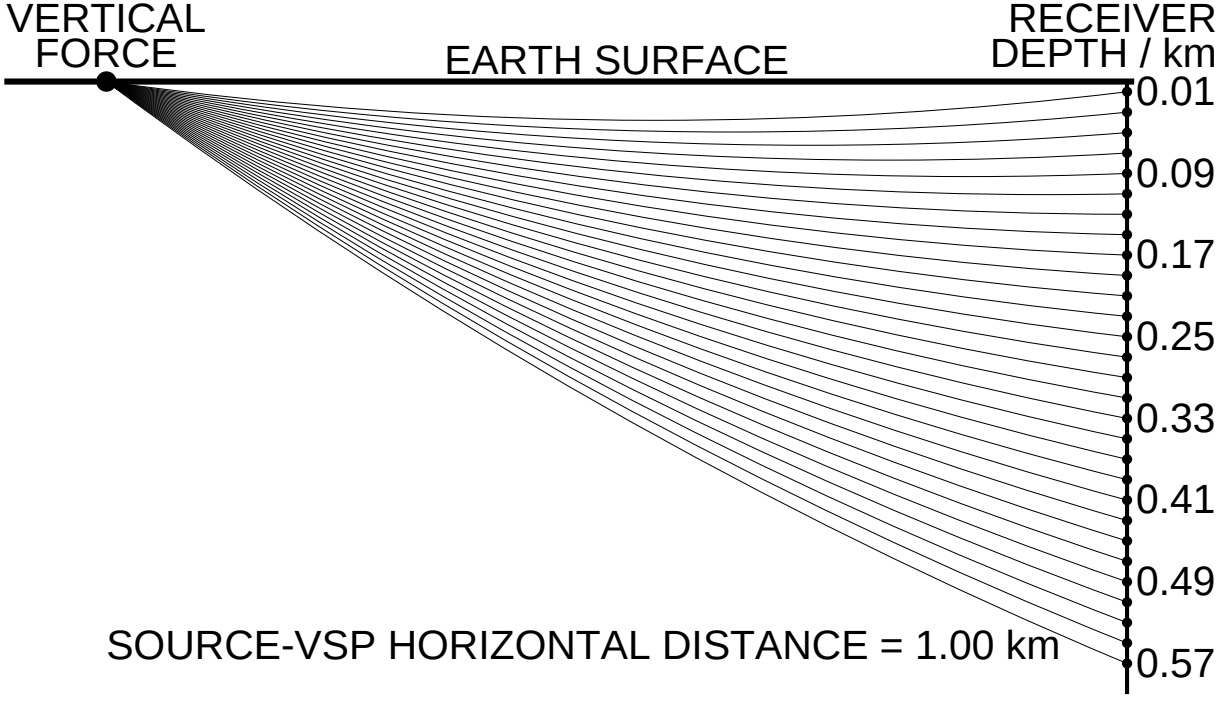

Model QI2, vertical component

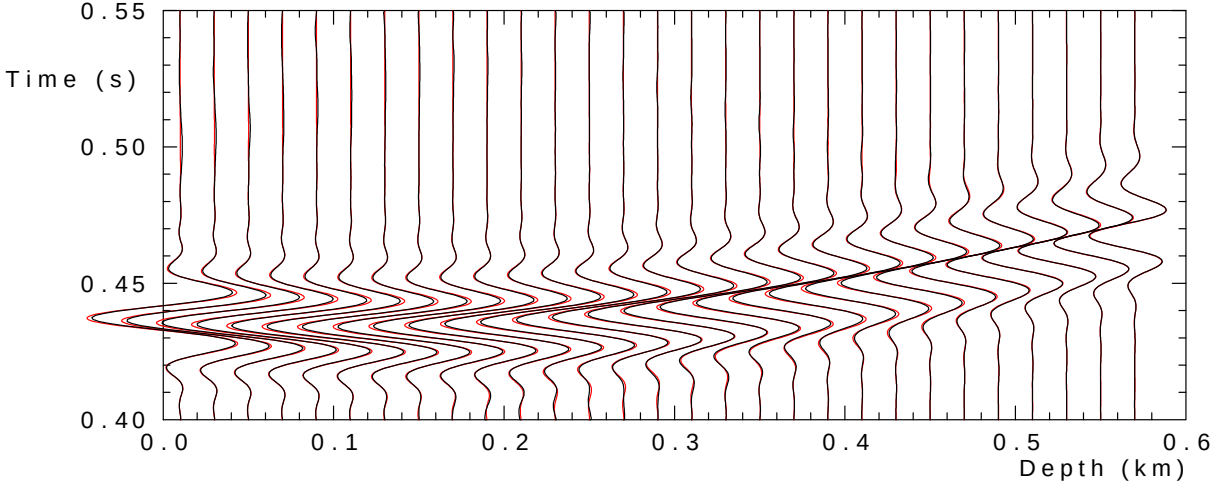

Anisotropic common S-wave reference rays.

Model QI2, vertical component

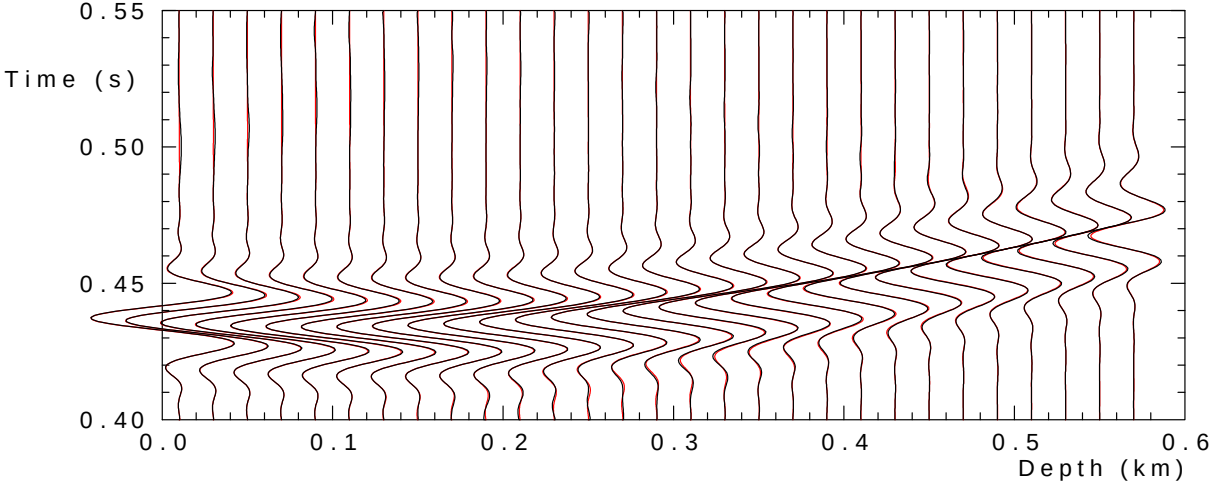

SH and SV reference rays.

Model QI2, radial component

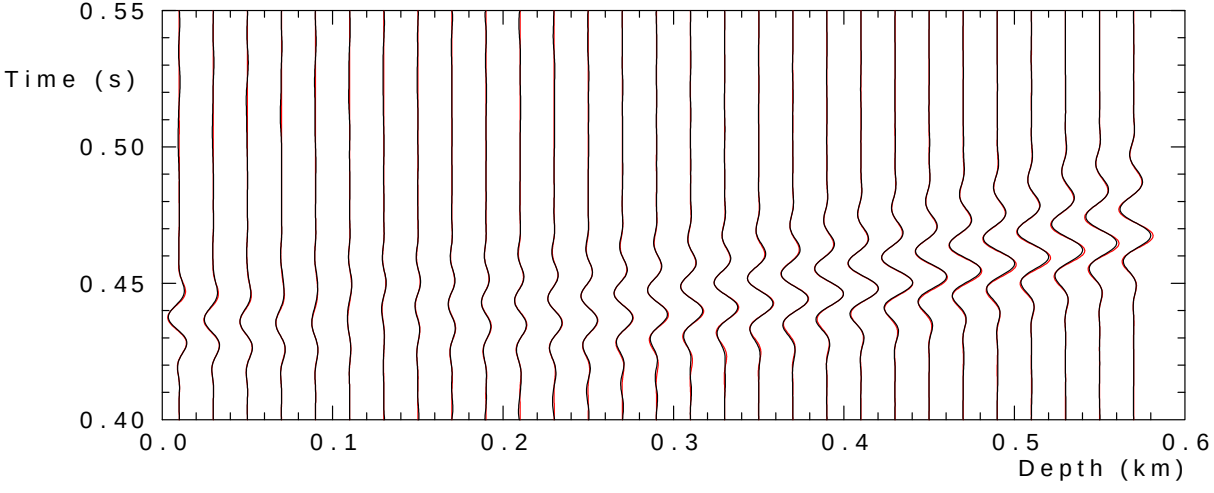

Anisotropic common S-wave reference rays.

Model QI2, radial component

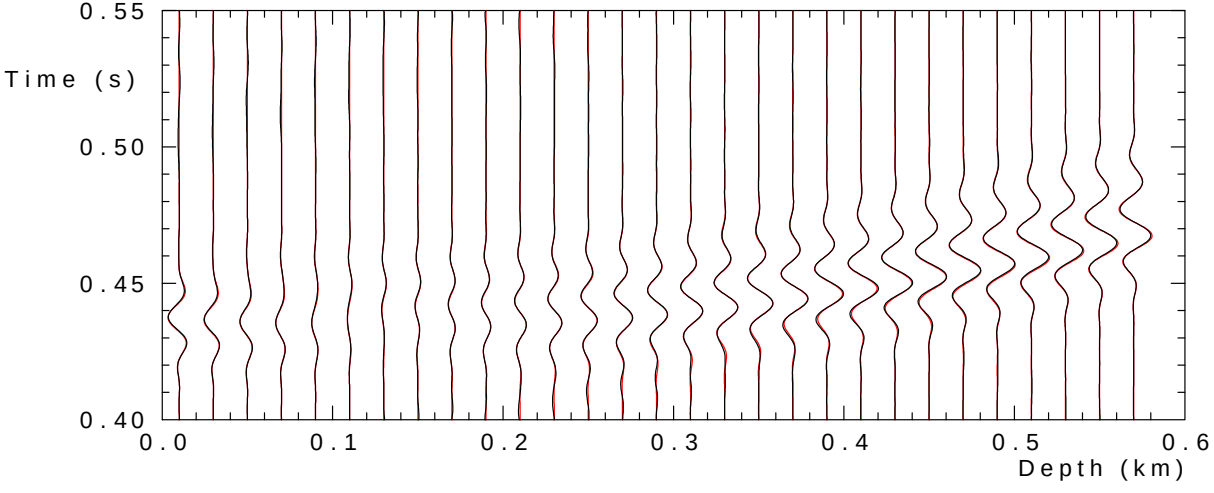

SH and SV reference rays.

Model QI2, transverse component

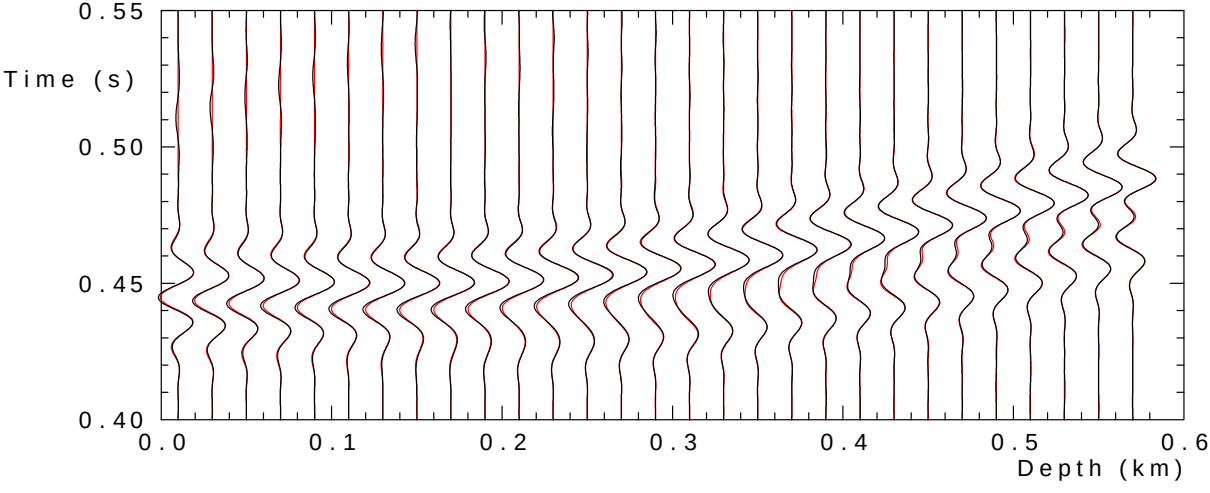

Anisotropic common S-wave reference rays.

Model QI2, transverse component

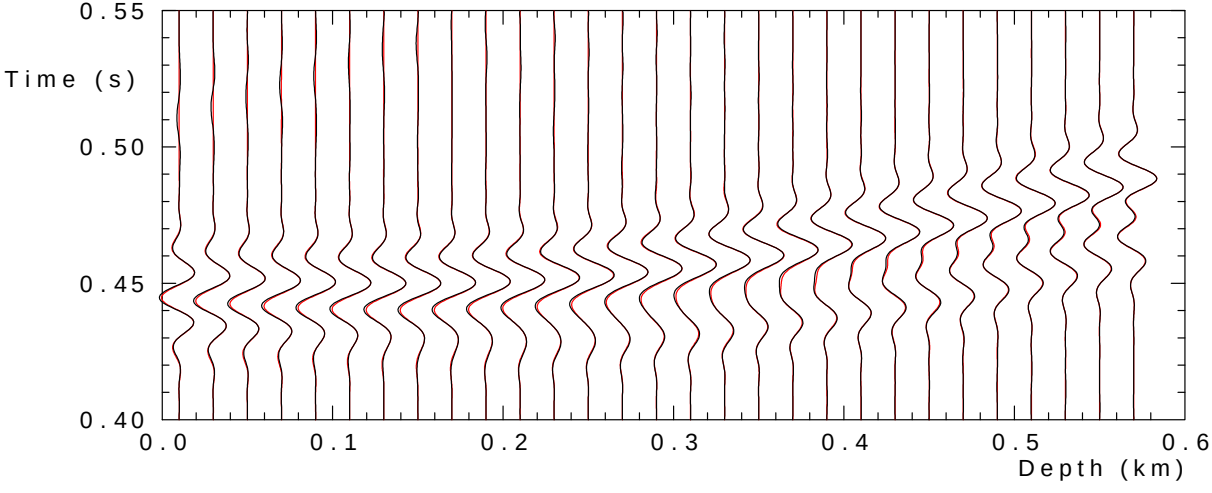

SH and SV reference rays.

Model QI4, vertical component

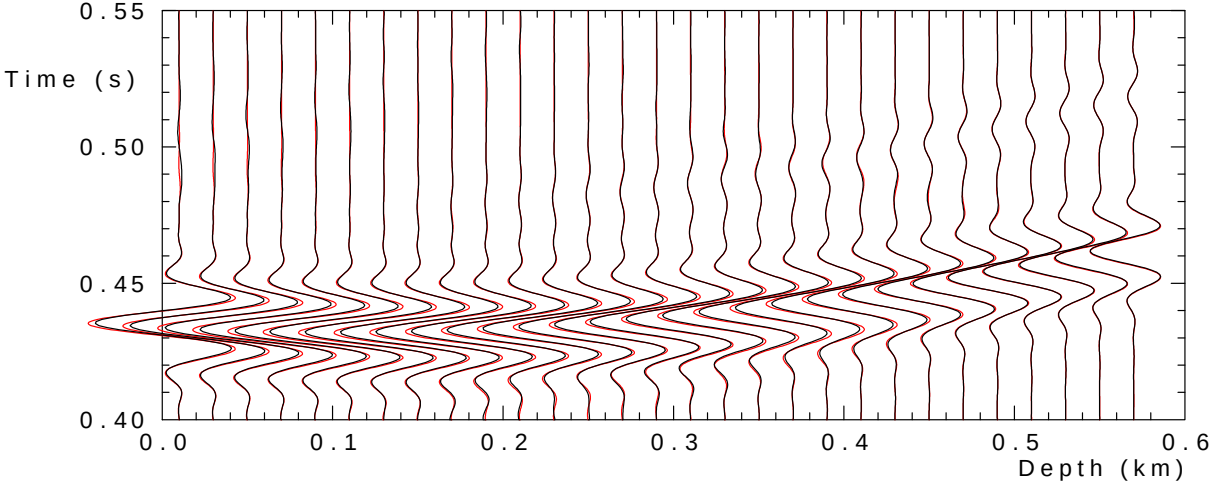

Anisotropic common S-wave reference rays.

Model QI4, vertical component

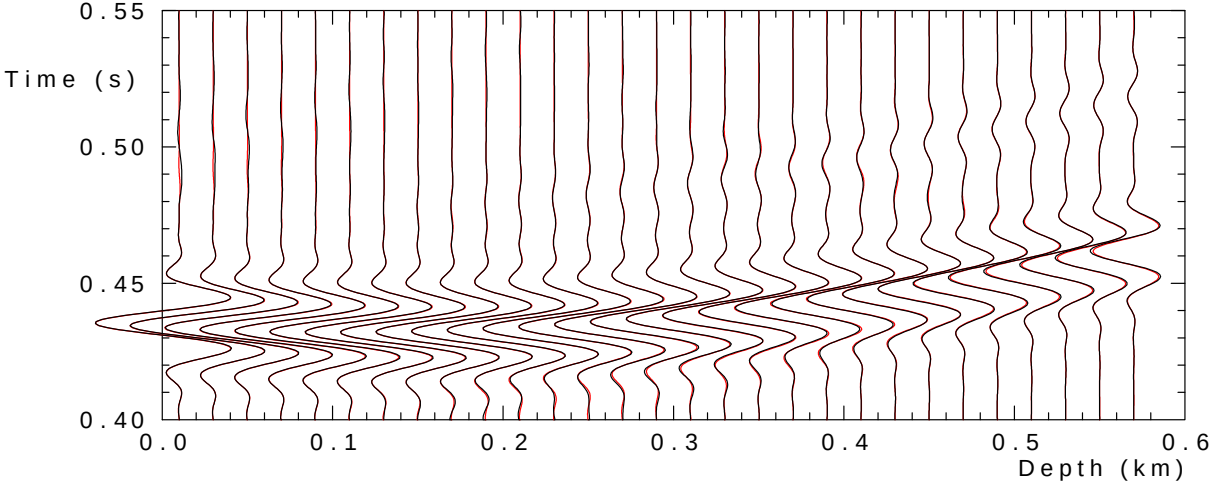

SH and SV reference rays.

Model QI4, radial component

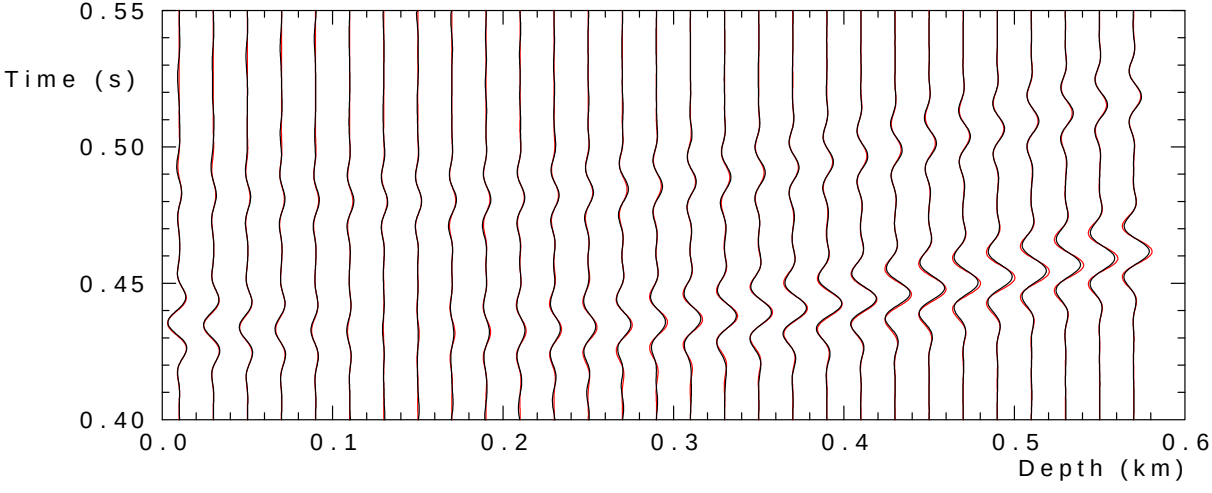

Anisotropic common S-wave reference rays.

Model QI4, radial component

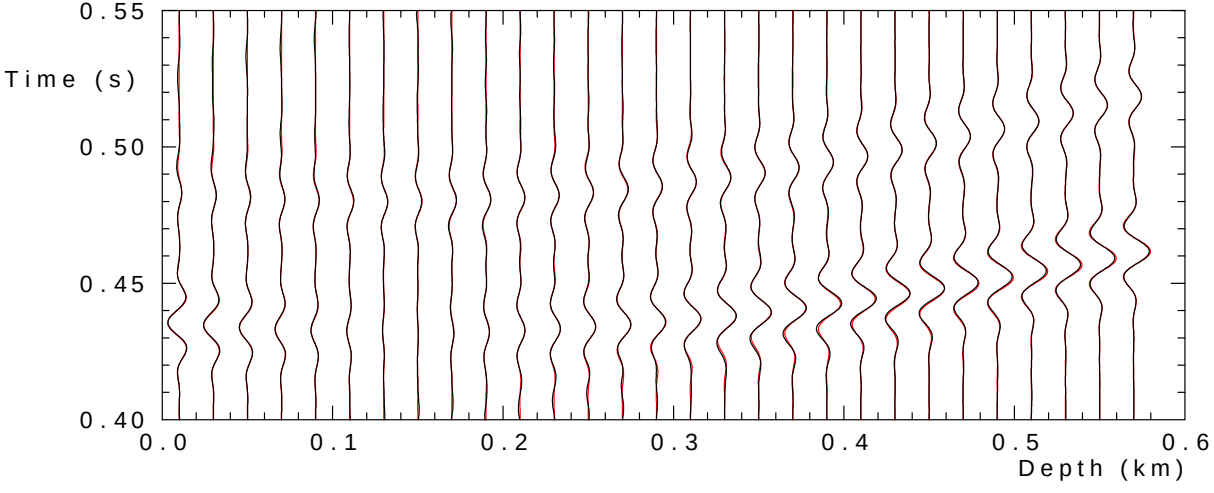

SH and SV reference rays.

Model QI4, transverse component

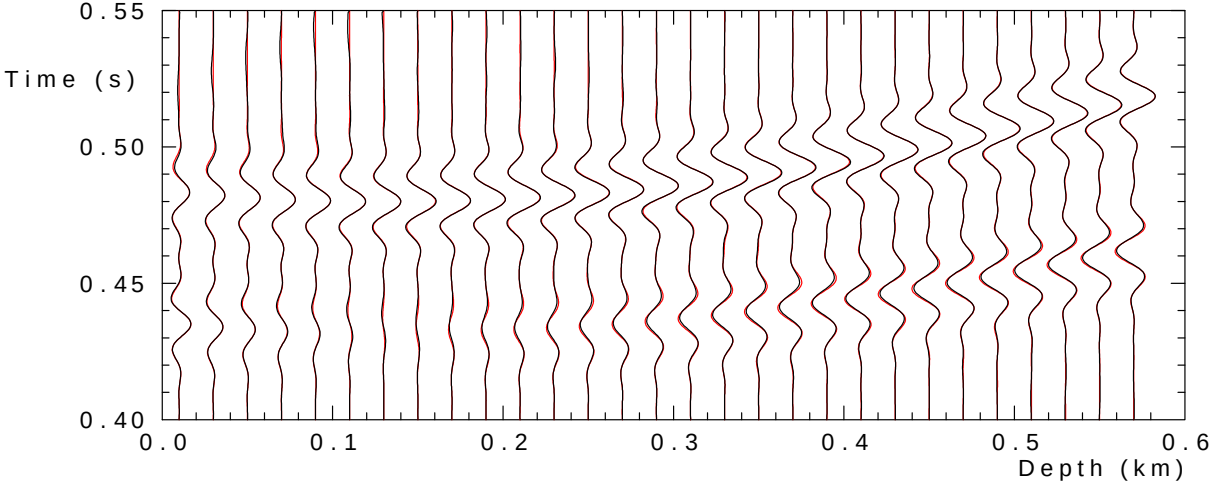

Anisotropic common S-wave reference rays.

Model QI4, transverse component

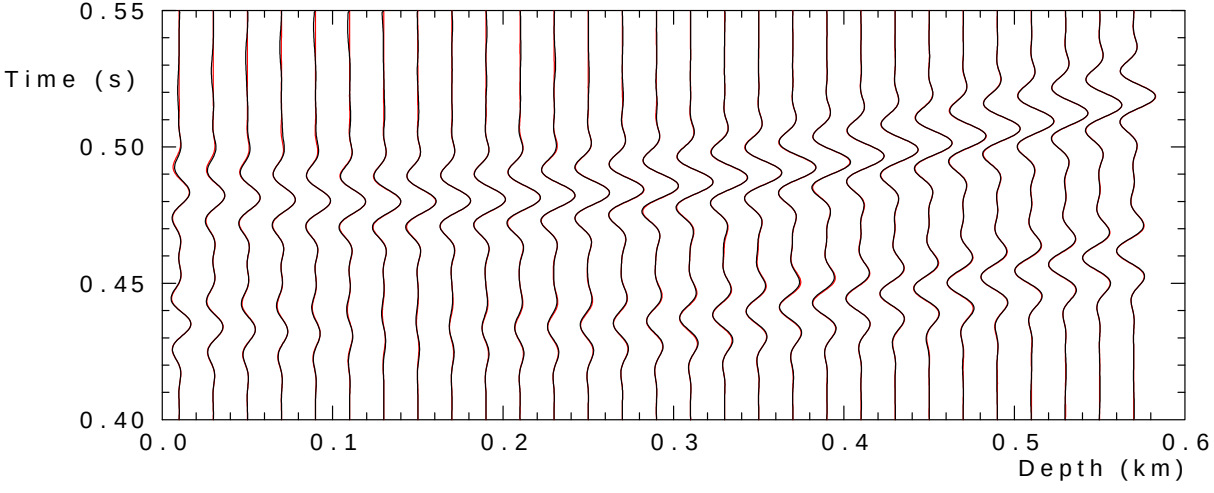

SH and SV reference rays.

Numerical comparison of seismograms in velocity models SC1_I and SC1_II (Klimeš & Bulant, 2015)

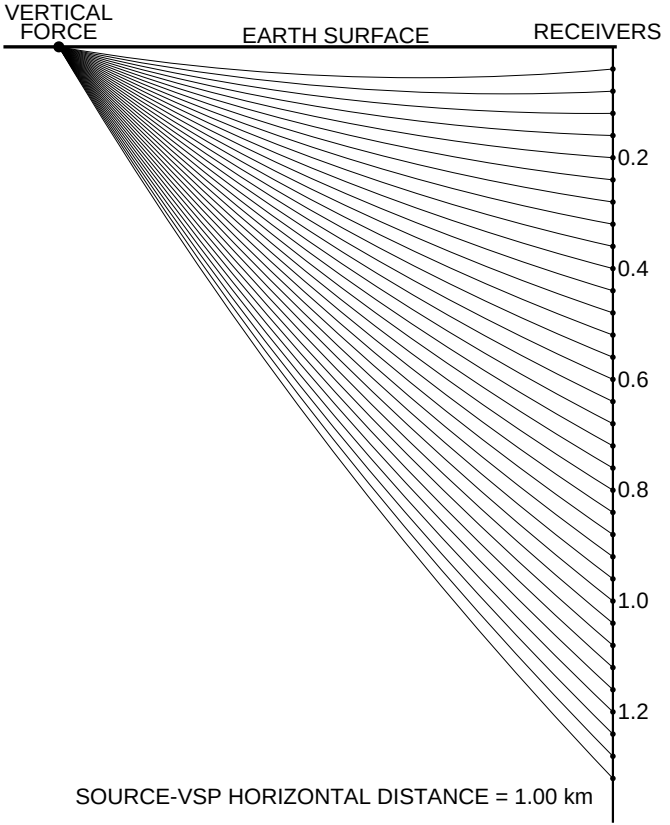

Model SC1_I, vertical component

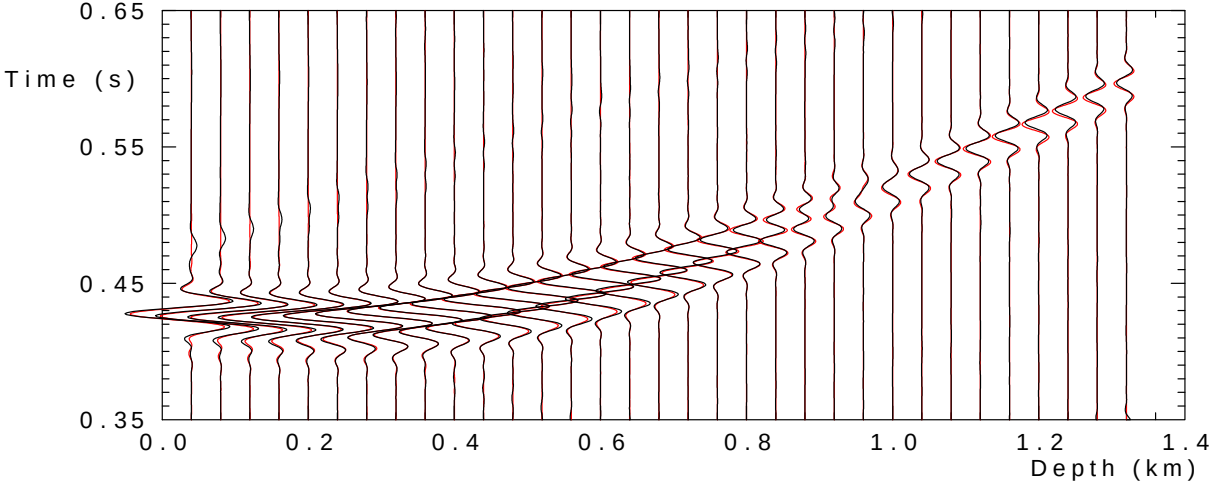

Anisotropic common S-wave reference rays.

Model SC1_I, vertical component

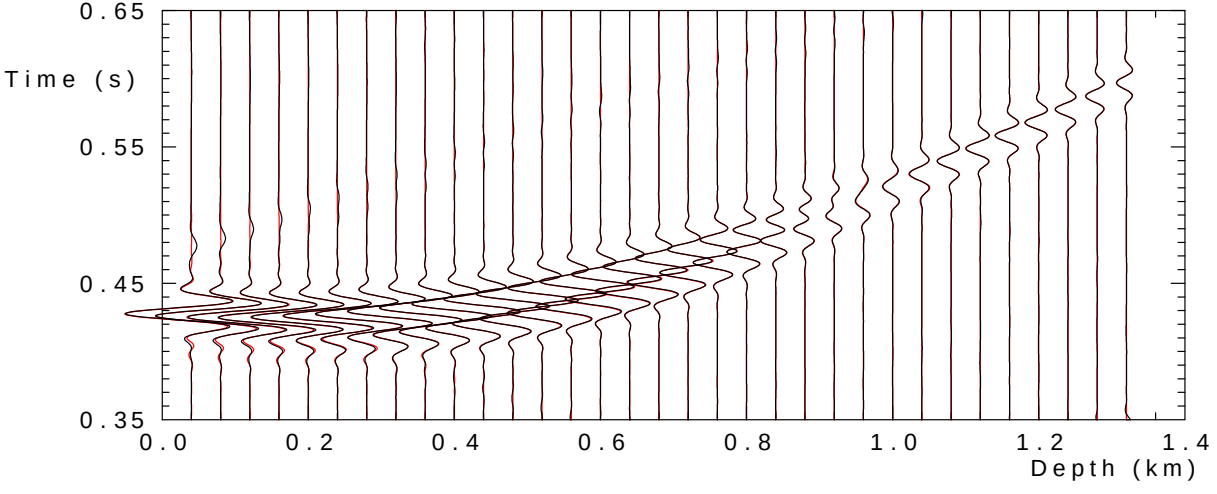

SH and SV reference rays.

Model SC1_I, radial component

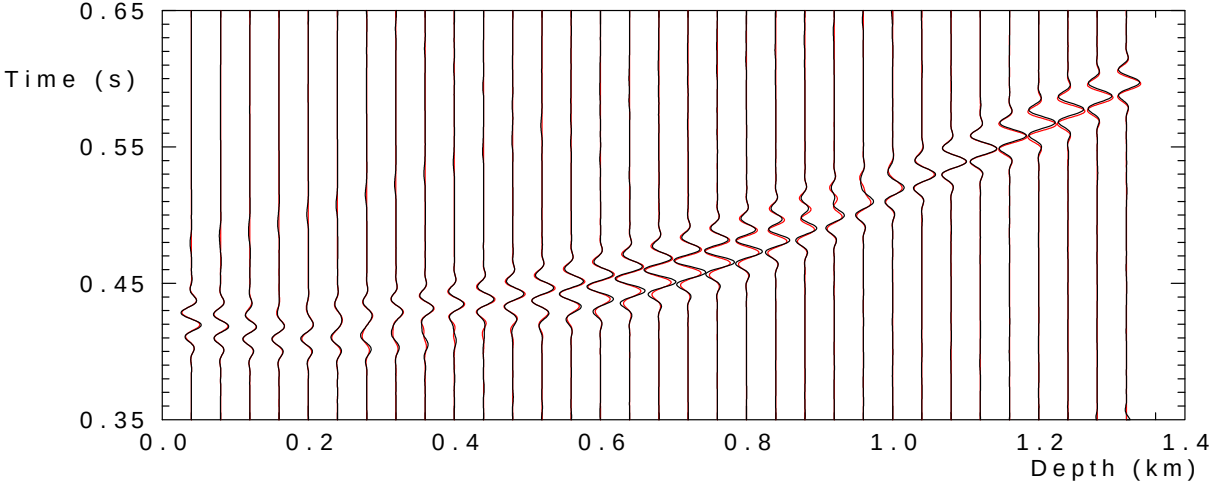

Anisotropic common S-wave reference rays.

Model SC1_I, radial component

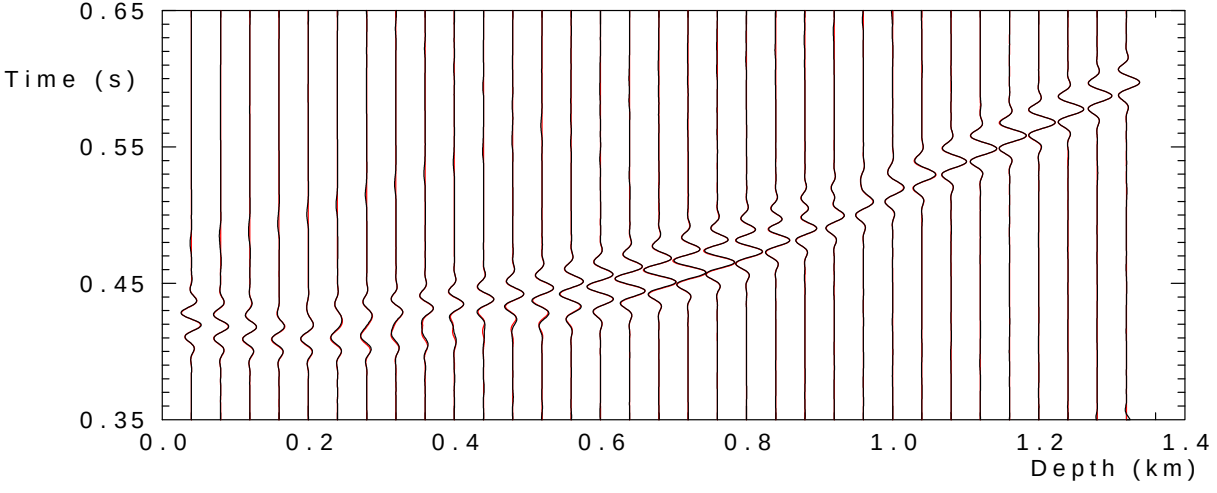

SH and SV reference rays.

Model SC1_I, transverse component

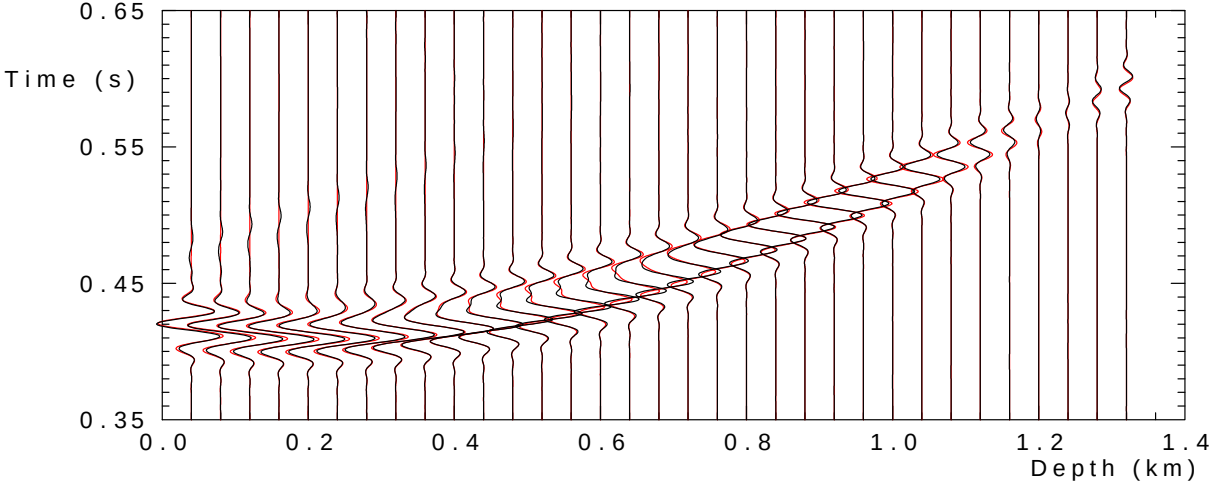

Anisotropic common S-wave reference rays.

Model SC1_I, transverse component

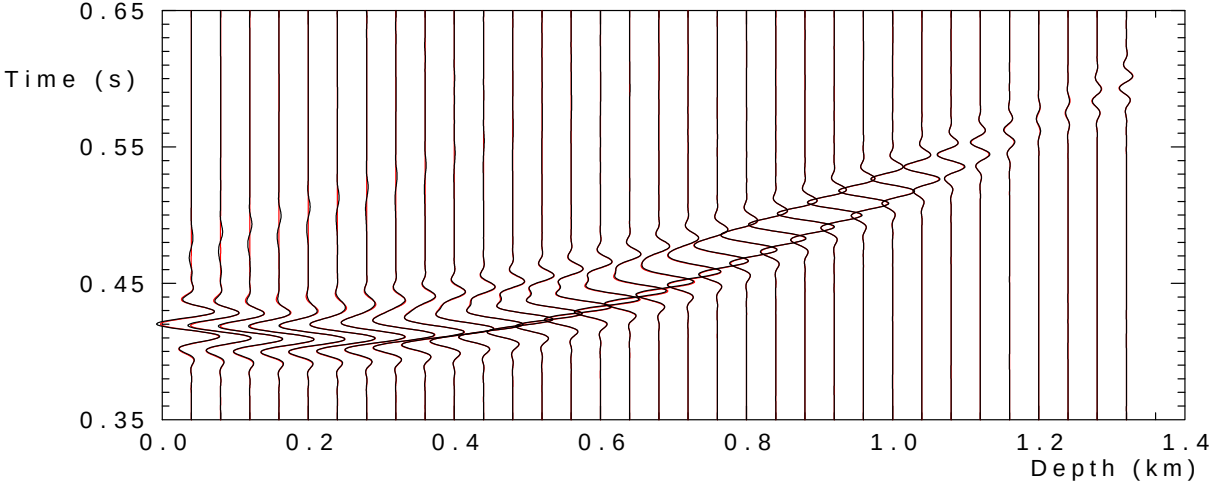

SH and SV reference rays.

Model SC1_II, vertical component

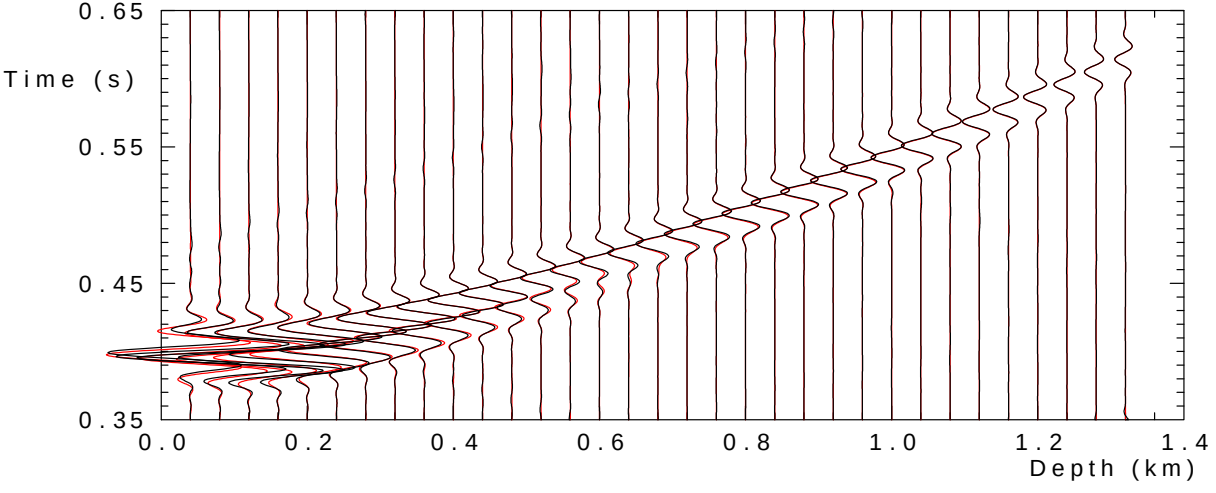

Anisotropic common S-wave reference rays.

Model SC1_II, vertical component

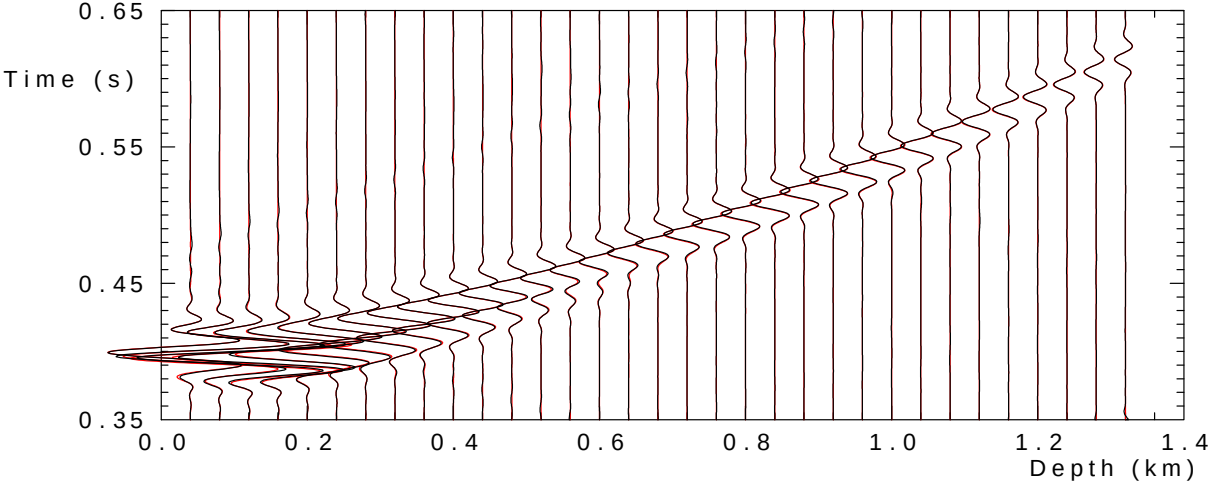

SH and SV reference rays.

Model SC1_II, radial component

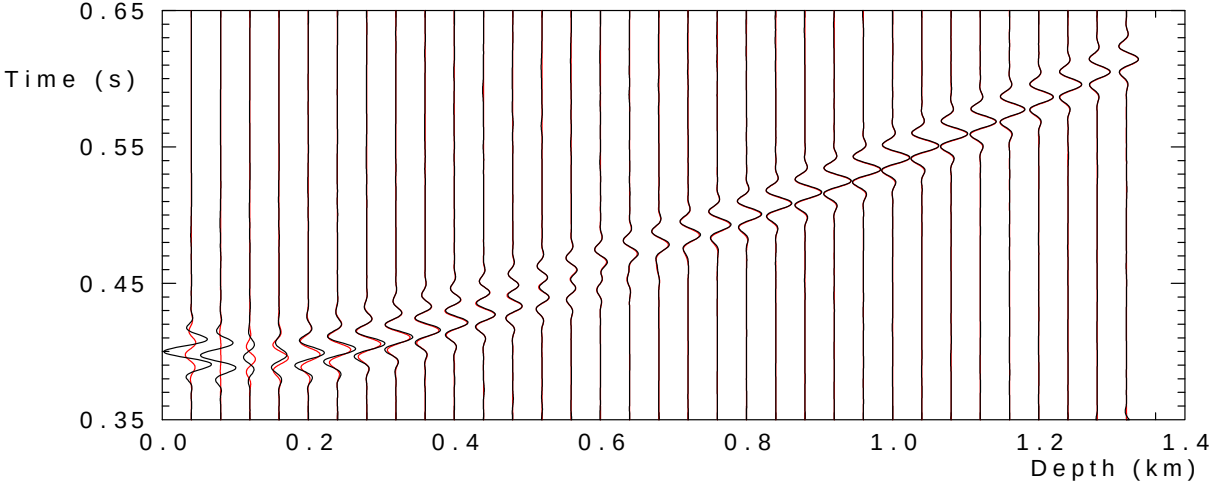

Anisotropic common S-wave reference rays.

Model SC1_II, radial component

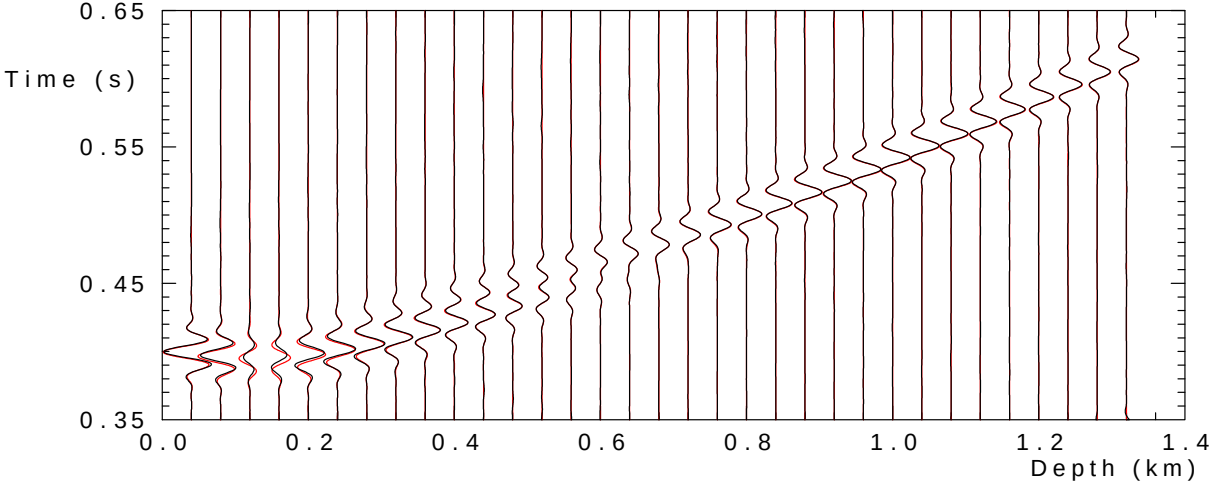

SH and SV reference rays.

Model SC1_II, transverse component

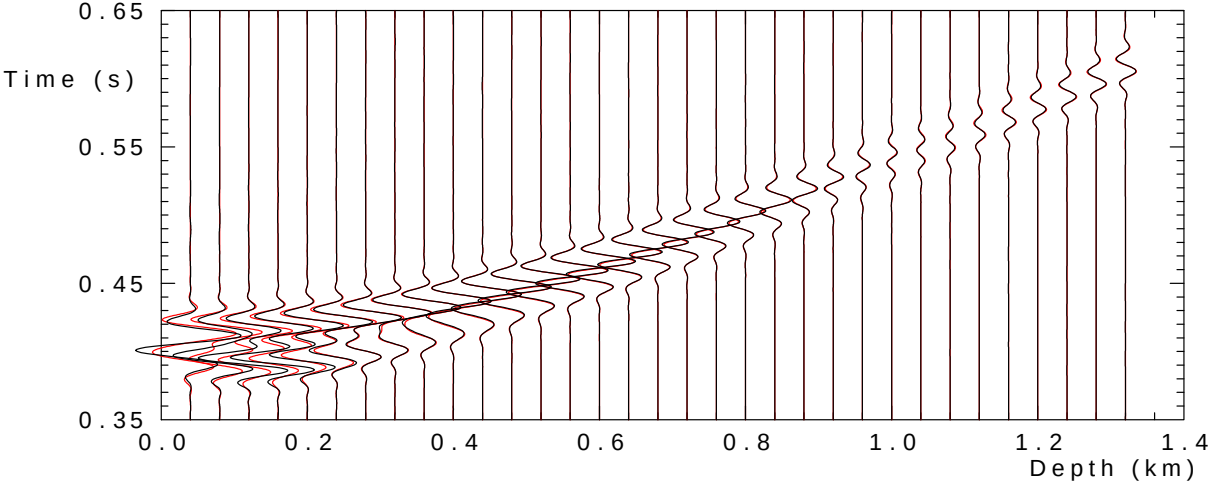

Anisotropic common S-wave reference rays.

Model SC1_II, transverse component

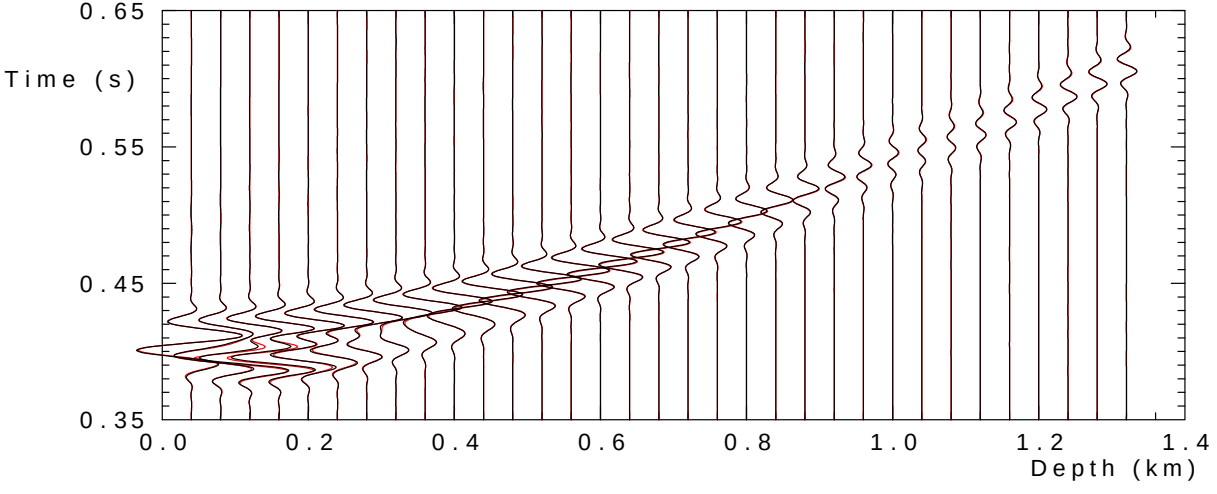

SH and SV reference rays.

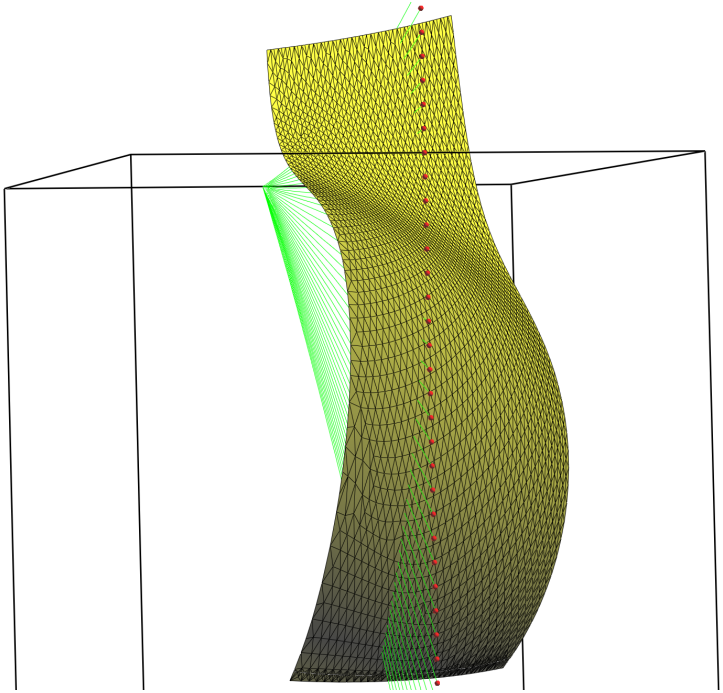

Two-point SV reference rays in velocity model SC1_II, together with a wavefront section triangulated according to the ray tubes. On the wavefront, we observe the belt of small geometrical spreading which intersects the receiver profile between the third and fourth receivers below the surface.

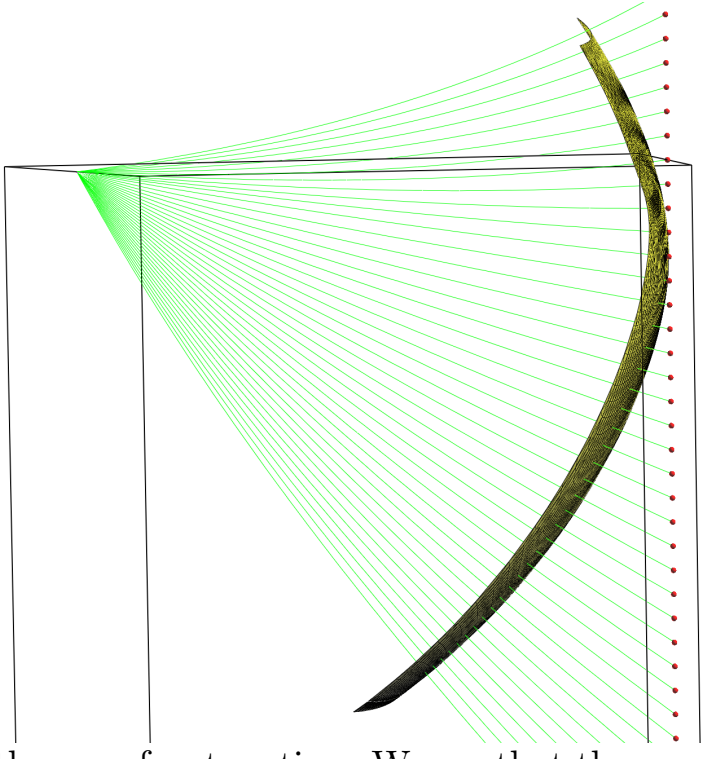

A side view of the wavefront section. We see that the wavefront is convex with just moderate variation of its curvature.

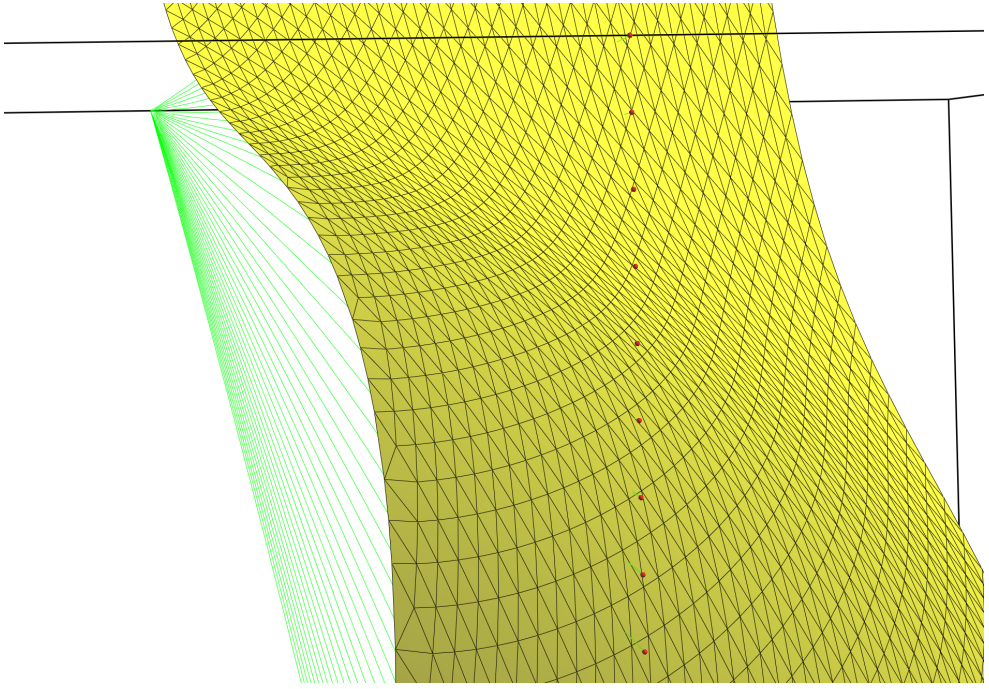

A detail of the wavefront section displaying the belt of small geometrical spreading which intersects the receiver profile between the third and fourth receivers below the surface. This belt probably causes the increase of the zero-order ray-theory amplitudes in comparison with the correct amplitudes, similarly as in the vicinity of caustics.

Coupling-ray-theory Gaussian beams

Fixing the remaining inaccuracy of the zero-order ray-theory amplitudes in velocity model SC1_II using the summation of the coupling-ray-theory Gaussian beams calculated along the SH and SV reference rays remains a challenge for our future research.

Outline

Introduction to the coupling ray theory for S waves

Prevailing-frequency approximation of the coupling ray theory

Reference rays for the coupling ray theory

Generally anisotropic medium which is approximately transversely isotropic

SH and SV reference rays in a generally anisotropic medium

Interpolation of the coupling-ray-theory Green function within ray cells

Conclusions

Interpolation of the ray-theory Green function within ray cells

Interpolation of the ray-theory Green function within ray cells using the algorithm designed by Bulant & Klimeš (1999) has been proved especially efficient for calculating the ray-theory Green function at the nodes of dense 3-D grids.

The discretized ray-theory Green function can be used for various applications including the ray-based Born approximation, non-linear determination of seismic hypocentres, studies of seismic sources, or Kirchhoff prestack depth migration.

The prevailing-frequency approximation enables us to interpolate the coupling-ray-theory S-wave Green function within ray cells using the algorithm designed by Bulant & Klimeš (1999).

Continuity of the coupling-ray-theory S-wave Green function along rays

Both prevailing-frequency coupling-ray-theory Green functions are calculated along a single anisotropic common S-wave reference ray. The anisotropic common reference rays then determine the ray cells for interpolation.

At each point of each reference ray, we have two prevailing-frequency coupling-ray-theory Green functions.

We double each reference ray and match the pair of the prevailing-frequency coupling-ray-theory Green functions with the pair of new rays so that each Green function is continuous along the corresponding new ray.

Continuity of the coupling-ray-theory S-wave Green function within ray tubes

In place of each reference ray, we have two new rays corresponding to two prevailing-frequency coupling-ray-theory Green functions. The Green function is continuous along the corresponding ray. As the result, each of three edges of each old ray tube is represented by two rays instead of one ray. We need to double each old ray tube and match the three pairs of edge rays with the pair of new ray tubes so that the Green function is continuous within either of the two new ray tubes.

The currently designed algorithm is obviously not optimal. The study of continuity of the prevailing-frequency coupling-ray-theory Green function within ray tubes represents the most challenging task.

Numerical examples of the interpolation within ray cells

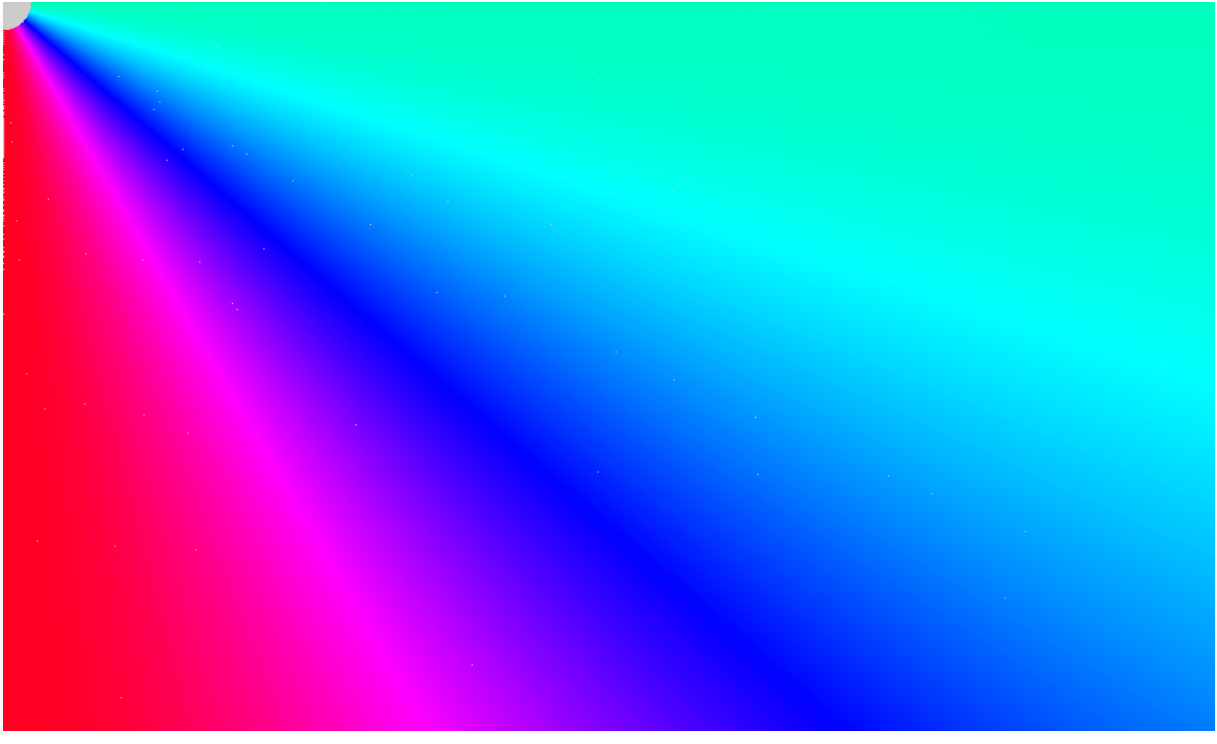

Relative coupling-ray-theory S-wave travel-time difference $|D/\overline{\tau}|$
in velocity model QIH.
Colour scale: 0.00%, 0.175%, 0.350%, 0.525%, 0.700%, 0.875%.

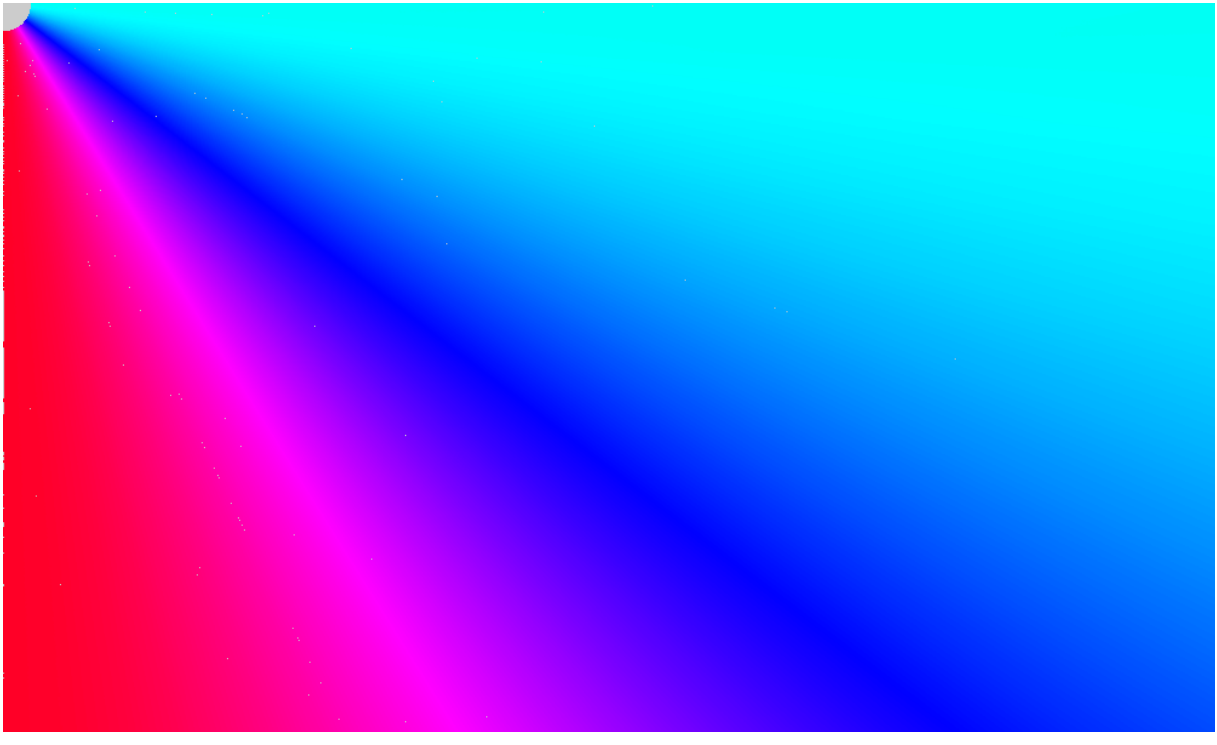

Relative coupling-ray-theory S-wave travel-time difference $|D/\overline{\tau}|$
in velocity model QI.
Colour scale: 0.00%, 0.35%, 0.70%, 1.05%, 1.40%, 1.75%.

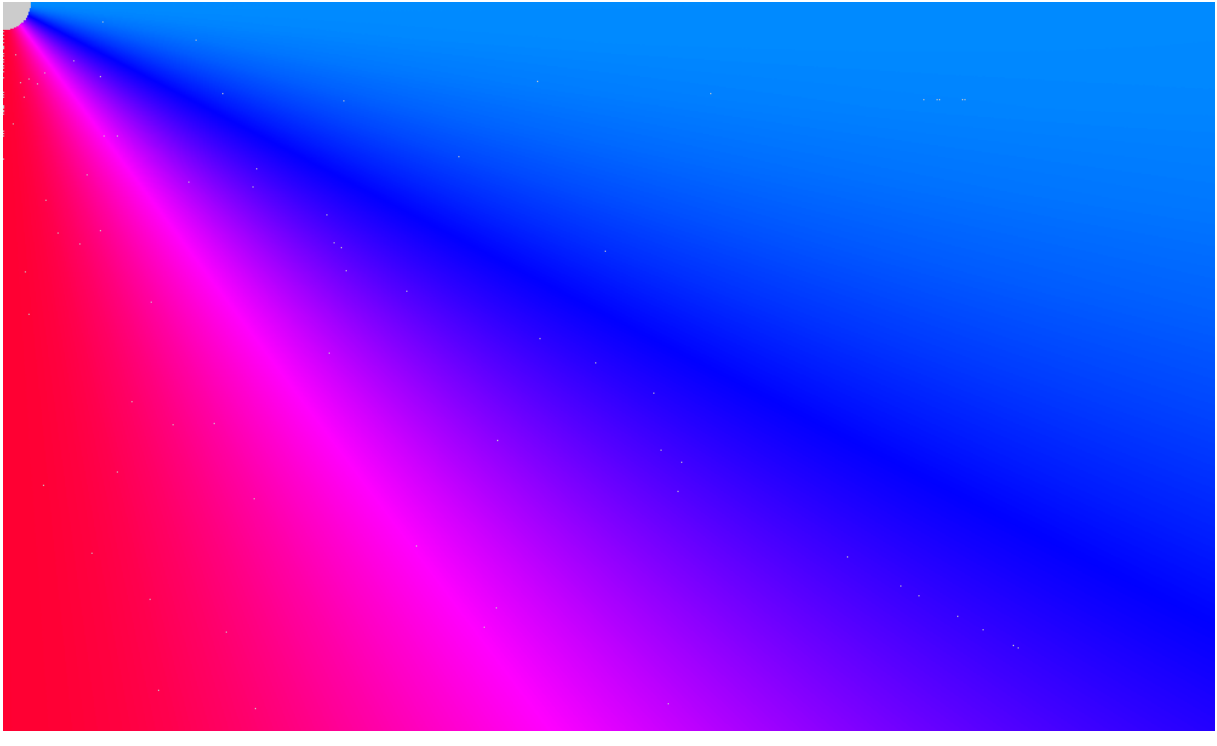

Relative coupling-ray-theory S-wave travel-time difference $|D/\overline{\tau}|$ in velocity model QI2.
Colour scale: 0.00%, 0.7%, 1.4%, 2.1%, 2.8%, 3.5%.

Relative coupling-ray-theory S-wave travel-time difference $|D/\overline{\tau}|$ in velocity model QI4.
Colour scale: 0.00%, 1.4%, 2.8%, 4.2%, 5.6%, 7.0%.

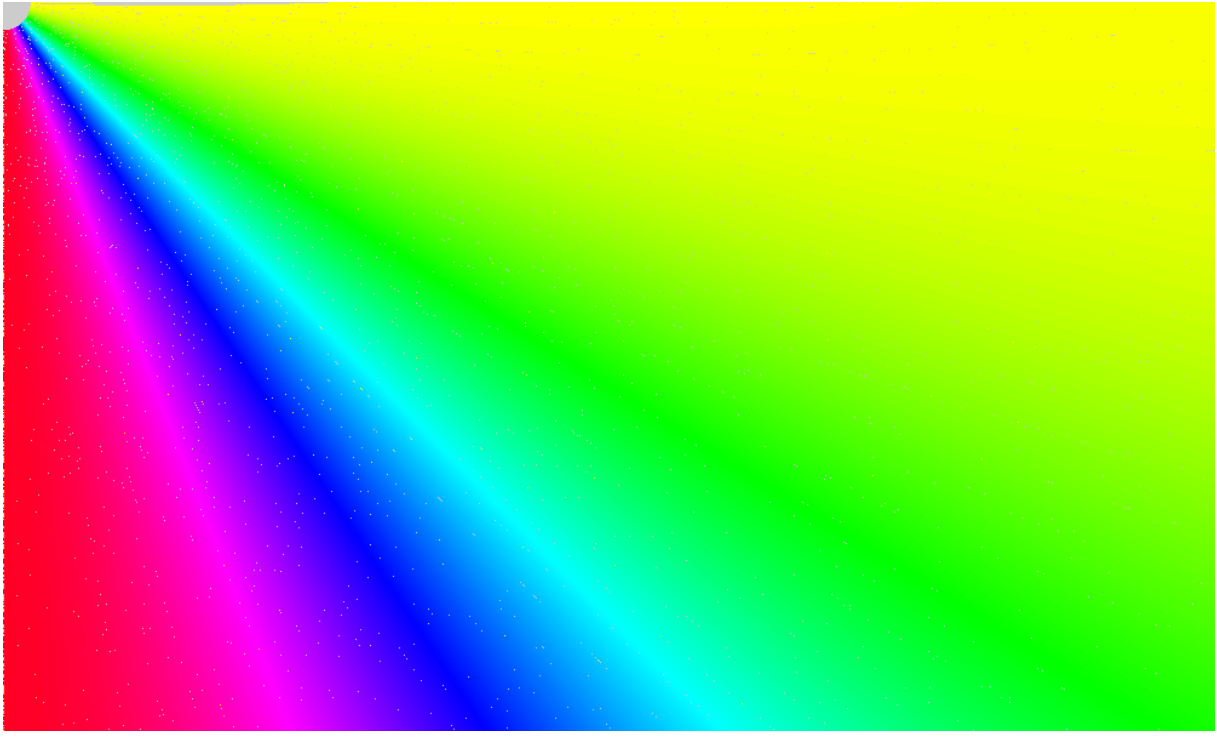

Relative coupling-ray-theory S-wave travel-time difference $|D/\overline{\tau}|$
in velocity model KISS.
Colour scale: 0.00%, 0.35%, 0.70%, 1.05%, 1.40%, 1.75%.

Relative coupling-ray-theory S-wave travel-time difference $|D/\overline{\tau}|$ in velocity model SC1_I.
Colour scale: 0.00%, 1.1%, 2.2%, 3.3%, 4.4%, 5.5%.

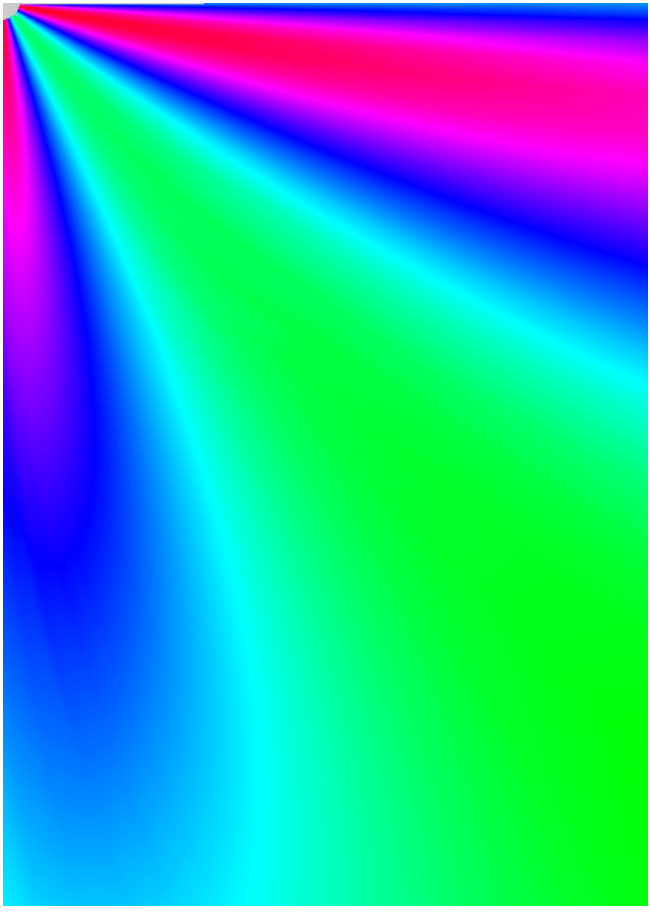

Relative coupling-ray-theory S-wave travel-time difference $|D/\overline{\tau}|$ in velocity model SC1_II.
Colour scale: 0.00%, 0.6%, 1.2%, 1.8%, 2.4%, 3.0%.

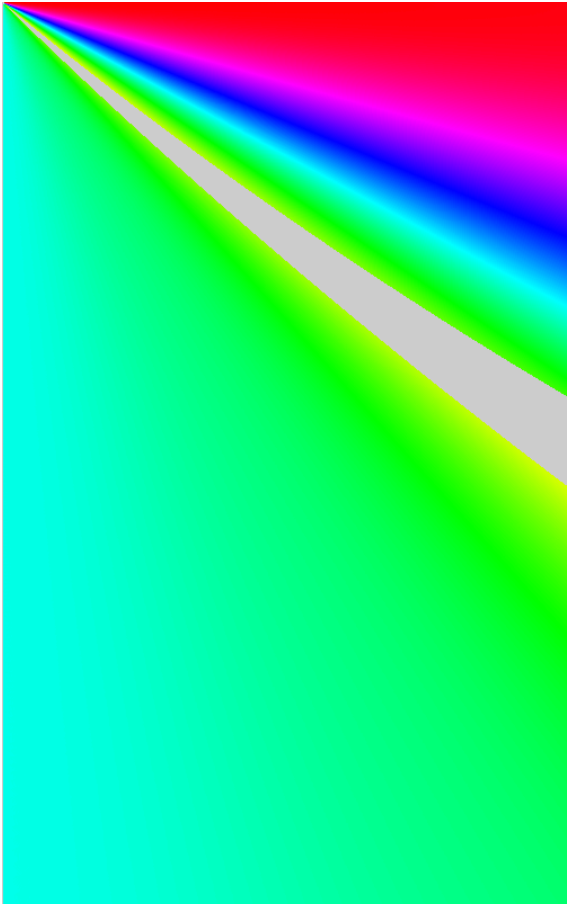

Relative coupling-ray-theory S-wave travel-time difference $|D/\overline{\tau}|$ in velocity model ORT. The diagonal shadow zone corresponds to the ray tubes which cannot be split into the pairs of tubes with continuous prevailing-frequency coupling-ray-theory Green functions. For infinitesimally short rays, the coupling-ray-theory polarization vectors approach the anisotropic-ray-theory polarization vectors which are discontinuous at a conical singularity. That is probably why the ray tubes in the vicinity of the conical singularity cannot be split into the pairs of tubes with continuous prevailing-frequency coupling-ray-theory Green functions.

Colour scale: 0.00%, 0.7%, 1.4%, 2.1%, 2.8%, 3.5%.

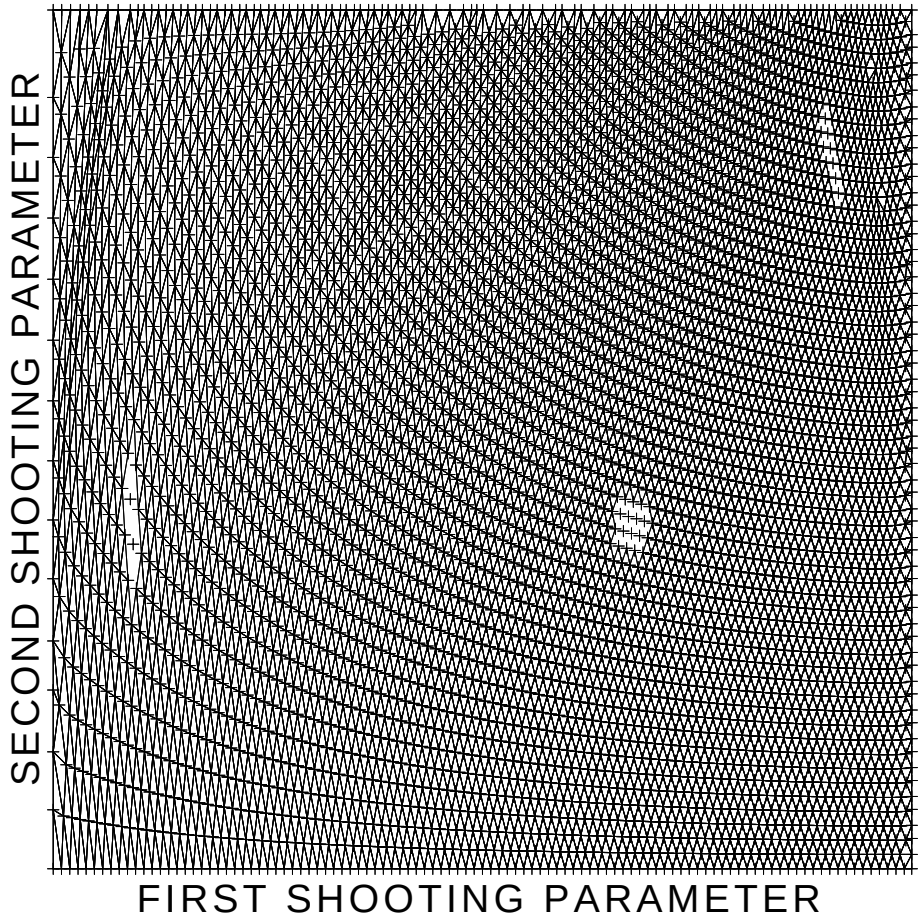

Ray tubes in velocity model ORT for the interpolation of coupling-ray-theory S-wave travel times.

Conclusions

The prevailing-frequency approximation of the coupling ray theory allows us to process the coupling-ray-theory wave field in the same way as the anisotropic-ray-theory wave field.

The prevailing-frequency approximation of the coupling ray theory can thus be included in wavefront tracing and in the interpolation within ray cells in anisotropic media. The most challenging task is the study of continuity of the prevailing-frequency coupling-ray-theory Green function within ray tubes and cells.

The interpolation within ray cells will enable common-source Kirchhoff prestack depth migration with coupling-ray-theory S waves.

In a generally anisotropic velocity model with a considerable transversely isotropic component, the SH and SV reference rays represent very accurate reference rays for the coupling ray theory. Otherwise, we should use the anisotropic common reference rays. We currently do not know any better reference rays then one of these two options.

References:

Bulant, P. & Klimeš, L. (1999): Interpolation of ray theory traveltimes within ray cells. *Geophys. J. int.*, **139**, 273–282.

Bulant, P. & Klimeš, L. (2002): Numerical algorithm of the coupling ray theory in weakly anisotropic media. *Pure appl. Geophys.*, **159**, 1419–1435.

Coates, R.T. & Chapman, C.H. (1990): Quasi-shear wave coupling in weakly anisotropic 3-D media. *Geophys. J. int.*, **103**, 301–320.

Klimeš, L. (2015): Determination of the reference symmetry axis of a generally anisotropic medium which is approximately transversely isotropic. *Seismic Waves in Complex 3-D Structures*, **25**, 177–185.

Klimeš, L. & Bulant, P. (2012): Single-frequency approximation of the coupling ray theory. *Seismic Waves in Complex 3-D Structures*, **22**, 143–167.

Klimeš, L. & Bulant, P. (2013): Interpolation of the coupling-ray-theory S-wave Green tensor within ray cells. *Seismic Waves in Complex 3-D Structures*, **23**, 203–218.

Klimeš, L. & Bulant, P. (2014): Prevailing-frequency approximation of the coupling ray theory for S waves along the SH and SV reference rays in a transversely isotropic medium. *Seismic Waves in Complex 3-D Structures*, **24**, 165–177.

Klimeš, L. & Bulant, P. (2014): Anisotropic-ray-theory rays in velocity model SC1_II with a split intersection singularity. *Seismic Waves in Complex 3-D Structures*, **24**, 189–205.

Klimeš, L. & Bulant, P. (2015): Ray tracing and geodesic deviation of the SH and SV reference rays in a heterogeneous generally anisotropic medium which is approximately transversely isotropic. *Seismic Waves in Complex 3-D Structures*, **25**, 187–208.

Klimeš, L. & Bulant, P. (2016): Prevailing-frequency approximation of the coupling ray theory for electromagnetic waves or elastic S waves. *Stud. geophys. geod.*, **60**, 419–450.

Pšenčík, I., Farra, V. & Tessmer, E. (2012): Comparison of the FORT approximation of the coupling ray theory with the Fourier pseudospectral method. *Stud. geophys. geod.*, **56**, 35–64.

Acknowledgements

The research has been supported:

by the Grant Agency of the Czech Republic under contracts P210/10/0736, 16-01312S and 16-05237S,

by the Ministry of Education of the Czech Republic within research project CzechGeo/EPOS LM2015079,

and by the consortium “Seismic Waves in Complex 3-D Structures”

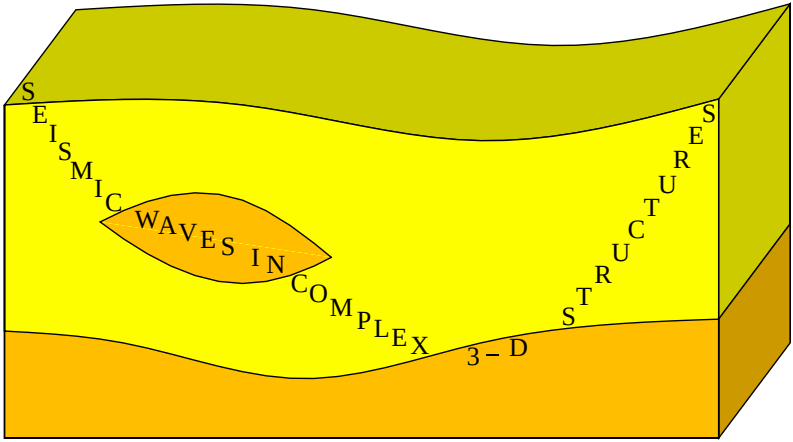

http://sw3d.cz